Department of Applied Physics

Exotic Vortex Structures in Dilute Bose-Einstein Condensates

Pekko Kuopanportti

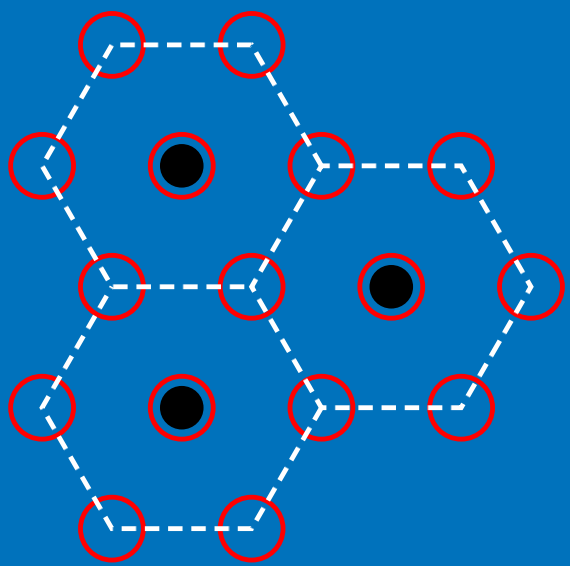

Aalto University

DOCTORAL DISSERTATIONS

Aalto University publication series
DOCTORAL DISSERTATIONS 118/2012

Exotic Vortex Structures in Dilute Bose-Einstein Condensates

Pekko Kuopanportti

Doctoral dissertation for the degree of Doctor of Science in Technology to be presented with due permission of the School of Science for public examination and debate in Auditorium K216 at the Aalto University School of Science (Espoo, Finland) on the 19th of October 2012 at 12 noon.

Aalto University
School of Science
Department of Applied Physics
Quantum Computing and Devices

Supervising professor
Prof. Risto Nieminen

Thesis advisor
Doc. Mikko Möttönen

Preliminary examiners
Prof. Mikio Nakahara, Kinki University, Japan
Dr. Tapio Simula, Monash University, Australia

Opponent
Prof. Brian P. Anderson, University of Arizona, USA

Aalto University publication series
DOCTORAL DISSERTATIONS 118/2012

ISBN 978-952-60-4784-3 (printed)
ISBN 978-952-60-4785-0 (pdf)
ISSN-L 1799-4934
ISSN 1799-4934 (printed)
ISSN 1799-4942 (pdf)
http://urn.fi/URN:ISBN:978-952-60-4785-0

Unigrafia Oy
Helsinki 2012

Finland

Publication orders (printed book):
pekko.kuopanportti@gmail.com

Aalto University

Abstract

Aalto University, P.O. Box 11000, FI-00076 Aalto www.aalto.fi

Author
Pekko Kuopanportti

Name of the doctoral dissertation
Exotic Vortex Structures in Dilute Bose-Einstein Condensates

Publisher School of Science

Unit Department of Applied Physics

Series Aalto University publication series DOCTORAL DISSERTATIONS 118/2012

Field of research Theoretical and Computational Physics

Manuscript submitted 12 June 2012 **Date of the defence** 19 October 2012

Permission to publish granted (date) 17 August 2012 **Language** English

☐ **Monograph** ☒ **Article dissertation (summary + original articles)**

Abstract

In 1995, atomic physics took a quantum leap with the experimental discovery of almost ideal Bose–Einstein condensation in dilute gases of alkali atoms. The gaseous condensates offer a rare chance to study an interacting many-particle system accurately from first-principles theories, and they can be used to simulate many seminal models that have proven elusive in their original context of, e.g., solid-state or high-energy physics. An important topic in the research has been the quantized vortex, which was experimentally realized in 1999 and whose existence is intimately related to the concepts of quantum phase coherence and superfluidity.

In this dissertation, unconventional vortex structures are investigated in the dilute condensates at ultralow temperatures. A combination of analytical and numerical methods is used to examine the structure, stability, and dynamical behavior of multiquantum vortices and vortex–antivortex pairs in spin-polarized condensates, unusual vortex lattices in two-species condensates, and spin textures in condensates with dipolar interactions. In studying the properties of the multiquantum vortices, particular emphasis is placed on exploring the practical limits of producing them through adiabatic pumping of vorticity. The majority of the research is conducted by solving the mean-field Gross–Pitaevskii and Bogoliubov equations.

Various original, experimentally verifiable results concerning the exotic vortex structures are presented. Novel splitting patterns of vortices with large quantum numbers are introduced, and it is shown that such vortices can be feasibly stabilized by piercing them with a focused laser beam. A recent experiment on vortex–antivortex pairs is simulated, and an excellent quantitative agreement with the experimental data is obtained. Unconventional ground-state vortex lattices, such as ones having a square geometry or consisting of two-quantum vortices, are shown to exist in rotating two-species condensates. Dipolar interactions are found to support helical spin-vortex states, and the energies of spin-wave excitations are observed to increase rapidly with the dipolar coupling strength.

This dissertation contributes to the understanding of superfluid phenomena in Bose–Einstein condensates and has significant implications for the prospects of detecting novel vortex structures in current experiments.

Keywords Bose-Einstein condensation, superfluidity, vortex

ISBN (printed) 978-952-60-4784-3 **ISBN (pdf)** 978-952-60-4785-0

ISSN-L 1799-4934 **ISSN (printed)** 1799-4934 **ISSN (pdf)** 1799-4942

Location of publisher Espoo **Location of printing** Helsinki **Year** 2012

Pages 66 **urn** http://urn.fi/URN:ISBN:978-952-60-4785-0

Tekijä
Pekko Kuopanportti

Väitöskirjan nimi
Eksoottiset vorteksirakenteet kaasumaisissa Bosen-Einsteinin kondensaateissa

Julkaisija Perustieteiden korkeakoulu

Yksikkö Teknillisen fysiikan laitos

Sarja Aalto University publication series DOCTORAL DISSERTATIONS 118/2012

Tutkimusala Teoreettinen ja laskennallinen fysiikka

Käsikirjoituksen pvm 12.06.2012 **Väitöspäivä** 19.10.2012

Julkaisuluvan myöntämispäivä 17.08.2012 **Kieli** Englanti

☐ **Monografia** ☒ **Yhdistelmäväitöskirja (yhteenveto-osa + erillisartikkelit)**

Tiivistelmä

Vuonna 1995 atomifysiikassa otettiin merkittävä edistysaskel, kun lähes ideaalinen Bosen–Einsteinin kondensaatio saavutettiin harvoissa alkaliatomikaasuissa. Atomikondensaatit mahdollistavat vuorovaikuttavan monihiukkassysteemin mallintamisen perusteorioihin nojaten. Kondensaattien avulla voidaan myös simuloida monia uraauurtavia malleja, joiden tutkiminen on osoittautunut hankalaksi niiden alkuperäisessä yhteydessä kuten kiinteän olomuodon tai korkean energian fysiikassa. Eräänä tärkeänä tutkimuskohteena on ollut kvantittunut virtauspyörre, vorteksi, joka tuotettiin kokeellisesti vuonna 1999. Vorteksit liittyvät läheisesti kvanttimekaanisen vaihekoherenssin ja suprajuoksevuuden käsitteisiin.

Väitöskirjassa tarkastellaan eksoottisia vorteksirakenteita harvoissa kondensaateissa nollalämpötilan rajalla. Analyyttisia ja laskennallisia menetelmiä käyttäen tutkitaan monikvantittuneiden vorteksien ja vorteksi–antivorteksiparien rakennetta, stabiilisuutta ja dynamiikkaa spinittömissä kondensaateissa, epätavallisia vorteksihiloja kahden kondensaatin systeemeissä sekä spin-tekstuureita kondensaateissa, joissa vaikuttavat dipoli–dipolivoimat. Monikvanttivorteksien tapauksessa halutaan erityisesti selvittää, kuinka suuria vorteksien kvanttilukuja voidaan saavuttaa niin sanotun vorteksipumpun avulla. Suurin osa tutkimuksesta perustuu Grossin–Pitaevskiin ja Bogoliubovin yhtälöiden ratkaisemiseen.

Työssä saavutetaan uusia, kokeellisesti varmistettavissa olevia tuloksia eksoottisiin vorteksirakenteisiin liittyen. Vortekseille, joiden kvanttiluku on suuri, löydetään uudenlaisia jakautumismekanismeja. Lisäksi osoitetaan, että tällaisista vortekseista saadaan dynaamisesti stabiileja lävistämällä niiden keskus fokusoidulla lasersäteellä. Vorteksi–antivorteksipareista suoritetaan simulaatioita, jotka tuottavat erinomaisen kvantitatiivisen vastaavuuden tuoreiden koehavaintojen kanssa. Kahden pyörivän kondensaatin systeemille löydetään epätavanomaisia perustiloja kuten neliömäisiä tai kaksikvanttivortekseista koostuvia vorteksihiloja. Dipoli–dipolivuorovaikutusten huomataan suosivan korkkiruuvimaisia spin-vorteksitiloja, ja spin-aaltojen eksitaatioenergioiden havaitaan kasvavan nopeasti dipoli–dipolivuorovaikutuksen voimakkuuden funktiona.

Väitöskirjassa esitetyt tulokset edistävät vorteksi-ilmiöiden tuntemusta Bosen–Einsteinin kondensaateissa. Tuloksilla on merkitystä myös, kun uusia vorteksirakenteita etsitään tämänhetkisissä kokeissa.

Avainsanat Bosen-Einsteinin kondensaatio, suprajuoksevuus, virtauspyörre, vorteksi

ISBN (painettu) 978-952-60-4784-3 **ISBN (pdf)** 978-952-60-4785-0

ISSN-L 1799-4934 **ISSN (painettu)** 1799-4934 **ISSN (pdf)** 1799-4942

Julkaisupaikka Espoo **Painopaikka** Helsinki **Vuosi** 2012

Sivumäärä 66 **urn** http://urn.fi/URN:ISBN:978-952-60-4785-0

Preface

This dissertation has been written as a result of the research carried out during the years 2009–2012 in the Quantum Computing and Devices group at the Department of Applied Physics in Aalto University School of Science. These years have been a splendid experience filled with constant changes, inspiring people, and unequaled personal growth. I will now take the opportunity to thank all the people who have helped and encouraged me during this time. In particular, the results presented in this dissertation would not exist without the dedication and team effort of my colleagues.

First of all, I would like to thank Prof. Risto Nieminen for supervising the dissertation and for the excellent working environment provided by the COMP Centre of Excellence. My instructor and the leader of the QCD group, Doc. Mikko Möttönen, deserves more credit than I can express in a few words. With his enthusiasm and deep physical intuition, he has guided me through my doctoral studies and taught me a great deal about quantum physics and the practices of the academic world, both of which can at times be quite perplexing. I am also greatly indebted to Dr. Jukka Huhtamäki, who has been invaluable as my postgraduate advisor, mentor, and collaborator. Many thanks belong to Dr. Ville Pietilä, M.Sc. Emmi Ruokokoski, Dr. Tapio Simula, and Dr. Sami Virtanen for the many educating and insightful discussions on Bose–Einstein condensates we have had in and out of the office. Moreover, I want to thank everyone else who has been a member of the QCD group during these years—in particular, Lic.Sc. Olli Ahonen, Dr. Ville Bergholm, M.Sc. Philip Jones, M.Sc. Juha Pirkkalainen, M.Sc. Juha Salmilehto, Dr. Paolo Solinas, Dr. Kuan Yen Tan, and M.Sc. Tuomo Tanttu—for making the group such a convivial place to work. During my time at the department, I have also enjoyed many discussions with M.Sc. Timo Hakkarainen, Doc. Ari

Harju, M.Sc. Miikka Heikkinen, M.Sc. Jaakko Hosio, Dr. Jussi Kajala, Dr. Jami Kinnunen, M.Sc. Aki Kutvonen, M.Sc. Juho Rysti, M.Sc. Olli-Pentti Saira, M.Sc. Topi Siro, and Dr. Eero Tölö. In addition, I want to acknowledge Dr. Emil Lundh for the fruitful collaboration on my first paper on Bose–Einstein condensates.

During the course of the work, I received financial support from the Vilho, Yrjö and Kalle Väisälä Foundation, the Emil Aaltonen Foundation, the KAUTE Foundation, and the Finnish Cultural Foundation. I am greatly indebted for their generosity. I acknowledge CSC – IT Center for Science Ltd. for computing resources as well as for the numerous courses I have attended at their premises.

I would like to thank my parents, Leena and Hannu, and my brother, Jaakko, for all their support and encouragement. Last but not least, I thank all my friends, many of whom I have already mentioned, for reminding me that life is more than just physics.

Now I guess I'll have to tell 'em
that I got no cerebellum.
Gonna get my Ph.D.
I'm a teenage lobotomy.
(Jeffrey Ross Hyman)

Helsinki, September 17, 2012,

Pekko Kuopanportti

Contents

List of Publications

This dissertation consists of an overview and of the following publications which are referred to in the text by their Roman numerals.

I P. Kuopanportti, E. Lundh, J. A. M. Huhtamäki, V. Pietilä, and M. Möttönen, *Core sizes and dynamical instabilities of giant vortices in dilute Bose–Einstein condensates*, Physical Review A **81**, 023603 (8 pages), February 2010.

II P. Kuopanportti and M. Möttönen, *Splitting dynamics of giant vortices in dilute Bose–Einstein condensates*, Physical Review A **81**, 033627 (8 pages), March 2010.

III P. Kuopanportti and M. Möttönen, *Stabilization and pumping of giant vortices in dilute Bose–Einstein condensates*, Journal of Low Temperature Physics **161**, 561–573 (13 pages), December 2010.

IV P. Kuopanportti, J. A. M. Huhtamäki, and M. Möttönen, *Size and dynamics of vortex dipoles in dilute Bose–Einstein condensates*, Physical Review A **83**, 011603(R) (4 pages), January 2011.

V P. Kuopanportti, J. A. M. Huhtamäki, and M. Möttönen, *Exotic vortex lattices in two-species Bose–Einstein condensates*, Physical Review A **85**, 043613 (7 pages), April 2012.

VI J. A. M. Huhtamäki and P. Kuopanportti, *Helical spin textures in dipolar Bose–Einstein condensates*, Physical Review A **82**, 053616 (7 pages),

November 2010.

VII J. A. M. Huhtamäki and P. Kuopanportti, *Elementary excitations in dipolar spin-1 Bose–Einstein condensates*, Physical Review A **84**, 043638 (6 pages), October 2011.

Author's Contribution

Publication I: "Core sizes and dynamical instabilities of giant vortices in dilute Bose–Einstein condensates"

The author contributed significantly to the main ideas of the work, implemented and performed all numerical simulations, analyzed the data, and wrote most of the manuscript.

Publication II: "Splitting dynamics of giant vortices in dilute Bose–Einstein condensates"

The author contributed substantially to the central ideas, implemented and performed the calculations, analyzed the data, and wrote the article.

Publication III: "Stabilization and pumping of giant vortices in dilute Bose–Einstein condensates"

The author carried out the analytical and numerical calculations for the work, analyzed the results, and prepared the manuscript.

Publication IV: "Size and dynamics of vortex dipoles in dilute Bose–Einstein condensates"

The author contributed signficantly to the main ideas of the research, performed approximately half of the numerical simulations, and wrote the paper.

Publication V: "Exotic vortex lattices in two-species Bose–Einstein condensates"

The author formulated the main ideas, performed the analytical and numerical calculations for the work, analyzed the results, and wrote the manuscript.

Publication VI: "Helical spin textures in dipolar Bose–Einstein condensates"

The author participated actively in developing the main ideas and contributed substantially to the preparation of the manuscript.

Publication VII: "Elementary excitations in dipolar spin-1 Bose–Einstein condensates"

The author participated actively in formulating the central ideas of the research and contributed significantly to the writing of the article.

1. Introduction

Superfluidity, superconductivity, and laser light may be considered among the most important discoveries of modern physics in terms of scientific interest and technological potential. Although these phenomena are observable on macroscopic length scales, their origin lies in quantum mechanics. In particular, all three are intimately related to the macroscopic occupation of a single quantum state.

The notion of macroscopic quantum occupation dates back to 1924–1925, when Albert Einstein extended Satyendra Nath Bose's statistical derivation of Planck's law for photons [1] to systems with a conserved number of particles [2, 3]. Einstein recognized that an ideal gas of atoms obeying the resulting statistical distribution would condense into the ground state of the system at sufficiently low temperatures. According to Einstein, a phase transition would occur at a critical temperature T_{c}, below which a macroscopic number of the atoms would occupy the lowest-energy quantum state. This phenomenon, which has subsequently been termed Bose–Einstein condensation, is a purely quantum-statistical phase transition in the sense that it occurs even for noninteracting bosons.

In 1938, Fritz London proposed that the then recently discovered superfluid ^{4}He [4,5] could be a manifestation of Bose–Einstein condensation [6, 7]. Although London's suggestion was later supported by neutron scattering experiments [8] and Monte Carlo simulations [9], the exact characteristics of the phase transition into the superfluid state still remain somewhat unclear due to strong interaction effects and the consequent lack of a transparent microscopic theory. In addition, Bose–Einstein condensation is closely related to the Bardeen–Cooper–Schrieffer (BCS) mechanism of superconductivity [10], which can be interpreted as the simultaneous formation and condensation of fermion pairs. However, the BCS superconductors are not well described by a simple Bose-gas picture since

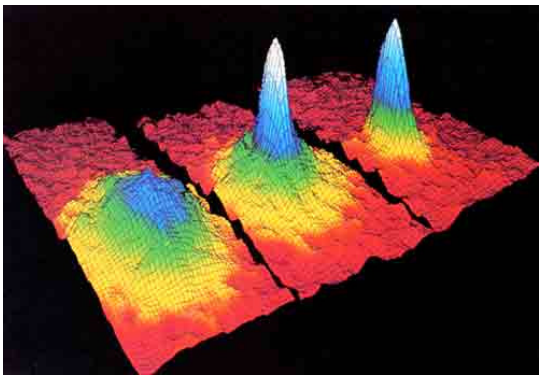

Figure 1.1. Successive occurrence of Bose–Einstein condensation in rubidium [16]. From left to right is shown the atomic distribution in the cloud just prior to condensation, at the start of condensation, and after full condensation. High peaks correspond to a large number of atoms. The distributions were recorded 6 ms after switching off the magnetic trap. Reprinted from The Nobel Foundation 9th October 2001 Press Release [19].

the fermion pairs behave as composite bosons only in an approximate sense [11].

In the 1960s, an intensive search began for Bose–Einstein condensation in dilute, weakly interacting bosonic gases, in which the condensation phenomenon would not be blurred by strong correlation effects or deviations from the exact Bose–Einstein statistics. After decades of research on trapping and cooling of neutral atoms [12–15], the final breakthrough came in 1995, when nearly ideal Bose–Einstein condensation was achieved in magnetically trapped ultracold vapors of alkali metals ^{87}Rb [16], ^{23}Na [17], and ^{7}Li [18] (see Fig. 1.1). These pioneering experiments—for which Eric Cornell, Wolfgang Ketterle, and Carl Wieman were later awarded the 2001 Nobel Prize in Physics [19]—launched an avalanche of research into the fascinating physics of dilute Bose–Einstein condensates (BECs). To date, the gaseous BECs have been experimentally realized by over a hundred groups.

To reach Bose–Einstein condensation in a dilute alkali gas, the atoms have to be cooled below the critical transition temperature $T_{\rm c}$. In a typical experiment, the number of atoms in the dilute BEC is of the order of 10^6 and the radius of the atomic cloud is of the order of 10–100 μm, yielding a particle density of roughly 10^{14} atoms/cm^3, which is by a factor 10^5 smaller than in air. Due to the low density, the condensation temperature is extremely low, typically of the order of $T_{\rm c} \approx 1$ μK. Such ultracold temperatures are usually achieved using a combination of different laser

cooling techniques and forced evaporative cooling [20–23]. To produce the atomic gas, alkali atoms are first evaporated off from a solid sample at high temperature. A beam of these atoms is directed into a so-called Zeeman slower in which the velocity of the atoms is reduced enough for the atoms to be captured in a magneto-optical trap. The gas is then typically laser-cooled down to sub-mK temperatures, after which it is cold enough to be captured using only magnetic fields. The final step is the evaporative cooling, in which the most energetic atoms are removed from the trap with radiofrequency transitions.

The gaseous condensates are in many ways exceptional compared with other systems exhibiting macroscopic quantum phenomena. On one hand, the interactions between the atoms give rise to nonlinear phenomena that are not present in laser fields. On the other hand, the interactions are sufficiently weak to allow high condensate fractions and a simple mean-field analysis, in contrast to superfluid helium. Due to their diluteness, the natural length scales in the condensates are relatively large, which makes them amenable to direct optical imaging. The ultracold gases have also turned out to be surprisingly robust and flexible. Diverse means to manipulate them—in particular the strength and spatial dependence of the atomic interactions [24]—render the gaseous condensates versatile tools for studying complex quantum phenomena in a controllable environment. The phenomena studied so far range from atom lasers [25–27] to quantum phase transitions [28, 29], but the condensates have been suggested to be used as simulators, e.g., for black holes [30, 31], cosmic strings [32], and self-gravitating gases [33].

The interplay between coherence, long-range order, and superfluidity are of fundamental interest in the study of BECs. The formation of long-range order in bosonic gases implies the onset of Bose–Einstein condensation and phase coherence. Conventionally, the characteristic features of superfluidity, i.e., dissipationless and irrotational flow, vanishing viscosity, and reduced moment of inertia, have also been interpreted in terms of phase coherence and spontaneous symmetry breaking: the superfluid system is described with an order parameter having a well-defined phase. Although superfluidity is indeed closely connected with the phase coherence of the system, it can still exist in the absence of a coherent BEC. On the other hand, the uniform ideal BEC is not a superfluid [34,35], and the degree to which the weak atomic interactions do sustain superfluidity in the atomic condensates has been a central issue under investigation.

Quantum phase coherence is typically manifested on microscopic length scales as the existence of quantized vortices which are string-like topological defects in the complex phase of the order-parameter field. Quantized vortices are characteristic of macroscopic quantum systems: these coherent whirlpools have been studied extensively in the context of superfluid helium [36,37] and superconductors [38], and they also appear in such diverse fields as astrophysics (neutron stars [39]), cosmology (cosmic strings [40]), optics (optical vortices [41]), and nuclear and elementary particle physics (rotating nuclei [42]).

Since quantized vortices are inherently connected with superfluidity, there has been wide interest in studying them in trapped dilute BECs [43]. Ever since their first experimental observation in 1999 by Matthews *et al.* [44], a plethora of vortex experiments in the dilute condensates have been providing important information on the coherence and superfluid properties of these systems.[1] A central issue has been the stability of vortices [46–56]—the existence of stable quantized vortices often serves as smoking-gun evidence for superfluidity.

The development of methods to trap neutral atoms by purely optical means [57,58] has made it possible to study BECs with internal spin degrees of freedom [59].[2] From the point of view of vortex physics, these spinor BECs are important since they exhibit a rich variety of unconventional topological defects such as half-quantum vortices [60–64], skyrmions [65], and monopoles [66–70]. The spin degrees of freedom can also be directly utilized to produce vortices either by magnetic manipulation [71] or by laser-induced artifical gauge fields [72]. In particular, the manipulation of the atomic spins by magnetic control fields allows for a cyclically operated vortex pump [73], which can, stability issues notwithstanding, produce giant vortices with arbitrarily large quantum numbers.

During the past few years, long-range dipole–dipole interactions between the condensate atoms have attracted a lot of interest [74]. Especially, recent experiments have indicated that the dipolar interactions can be relevant for some phenomena in spinor condensates of ^{87}Rb [75,76]. The dipole–dipole interactions also play a role in the study of topological defects, since dipolar forces are able to stabilize spin vortices [77–80] and may give rise to intriguing spin textures such as spin helices [81].

[1] For an almost exhaustive list of experiments on vortices in BECs, see Ref. [45].
[2] When the atoms are trapped using magnetic fields, their spins become polarized along the field direction and the spin degree of freedom is effectively frozen out.

The objective of this dissertation is to study exotic vortex structures in gaseous BECs at ultralow temperatures. A combination of numerical and analytical methods is used to examine the structure, stability, and dynamical behavior of multiply quantized vortices and vortex–antivortex pairs in spin-polarized BECs, unconventional vortex lattices in two-species condensates, and spin textures in dipolar BECs. The underlying purpose of these investigations is to broaden and deepen our understanding of vortex phenomena in the gaseous condensates. Although the research is theoretical, it is strongly motivated by current experimental prospects. For example, when studying the stability of multiply quantized vortices, particular emphasis is placed on analyzing the aforementioned vortex pump and exploring its practical limits in producing giant vortices with extremely large quantum numbers. Also, the investigation of vortex–antivortex pairs is closely related to recent experiments [82].

This overview is organized as follows. Chapter 2 describes the physical systems considered in the dissertation and the theoretical framework used to model them. Chapters 3–5 review the research reported in Publications I–VII: Quantized vortices, topological methods to create them, and the stability of vortices with large quantum numbers (Publications I–III) are discussed in Chapter 3. Vortex–antivortex pairs in spin-polarized BECs (Publication IV) and vortex lattices in a system of two interacting condensates (Publication V) form the topic of Chapter 4. In Chapter 5, BECs with dipolar interactions are introduced, and helical spin textures and elementary excitations in such systems (Publications VI and VII) are investigated. Each of Chapters 3–5 also includes a motivation for studying the topic at hand and a discussion of the obtained results. Finally, Chapter 6 concludes the dissertation by summarizing the contributions made and proposing areas for future research.

2. Mean-Field Theory of Dilute Bose–Einstein Condensates

In this chapter, we describe the mean-field theory used to model the dilute BECs at ultralow temperatures [23, 83, 84]. In Sec. 2.1, we characterize the second-quantized Hamiltonian of the system, and in Sec. 2.2, we define Bose–Einstein condensation using the Penrose–Onsager criterion. Section 2.3 introduces the nonlinear differential equation governing the time evolution of the condensate, the Gross–Pitaevskii equation, and Sec. 2.4 discusses elementary excitations and their role in the stability analysis of the condensate.

2.1 System characterization and Hamiltonian

The physical system considered in this dissertation is an ultracold gas of weakly interacting bosonic atoms which are captured, manipulated, and measured using magnetic and laser fields. Alkali-metal atoms are particularly suitable for such purposes since their optical transitions can be excited with available lasers and their energy-level structure enables laser cooling to record-low temperatures [85]. The atoms are assumed to have a hyperfine spin $F = 1$, giving rise to a three-component quantum field operator describing them. In the z-quantized basis $|F = 1, j\rangle$, the field operator has the components $\hat{\psi}_j(\mathbf{r}, t)$, where $j \in \{1, 0, -1\}$.[1]

The effective grand-canonical Hamiltonian $\hat{K}$ of the system is written

[1] The hyperfine spin F is the quantum number corresponding to the total angular momentum operator $\mathbf{F} = \mathbf{I} + \mathbf{J}$, where $\mathbf{I}$ and $\mathbf{J}$ are the operators for the nuclear spin and the electronic angular momentum, respectively, in units of $\hbar$. For the experimentally most relevant alkali atoms ^{23}Na and ^{87}Rb, the corresponding quantum numbers have the values $I = 3/2$ and $J = 1/2$, which implies $F = 1$ or $F = 2$, the first being the lower-energy multiplet [86, 87]. The $F = 1$ multiplet is fully characterized by the z-quantized basis states $|F = 1, j\rangle$, where $j \in \{1, 0, -1\}$ is the eigenvalue of the z component of $\mathbf{F}$.

as [88, 89]

$$\begin{aligned}\hat{K} &= \hat{H} - \mu\hat{N} = \int \mathrm{d}^3 r \Big[\hat{\psi}_j^\dagger(\mathbf{r},t) \left(\mathcal{H}_{jk} - \mu\delta_{jk}\right) \hat{\psi}_k(\mathbf{r},t) \\ &+ \frac{g_\mathrm{n}}{2} \hat{\psi}_j^\dagger(\mathbf{r},t) \hat{\psi}_{j'}^\dagger(\mathbf{r},t) \hat{\psi}_{j'}(\mathbf{r},t) \hat{\psi}_j(\mathbf{r},t) \\ &+ \frac{g_\mathrm{s}}{2} \hat{\psi}_j^\dagger(\mathbf{r},t) \hat{\psi}_{j'}^\dagger(\mathbf{r},t) \mathbf{F}_{jk} \cdot \mathbf{F}_{j'k'} \hat{\psi}_{k'}(\mathbf{r},t) \hat{\psi}_k(\mathbf{r},t) \Big], \end{aligned} \tag{2.1}$$

where μ is the chemical potential controlling the average number of particles. The single-particle Hamiltonian operator is given by

$$\mathcal{H}_{jk} = \left[-\frac{\hbar^2\nabla^2}{2m} + V_\mathrm{tr}(\mathbf{r}) \right] \delta_{jk} + g_F \mu_\mathrm{B} \mathbf{B}(\mathbf{r},t) \cdot \mathbf{F}_{jk}, \tag{2.2}$$

where m denotes the atomic mass, g_F is the Landé g-factor, and μ_B is the Bohr magneton. The possibly present external magnetic field is denoted by $\mathbf{B}(\mathbf{r},t)$, and $V_\mathrm{tr}(\mathbf{r}) = m\left(\omega_r^2 x^2 + \omega_r^2 y^2 + \omega_z^2 z^2\right)/2$ is the optical potential trapping the atoms. Moreover, $\mathbf{F} = F^x\,\hat{\mathbf{x}} + F^y\,\hat{\mathbf{y}} + F^z\,\hat{\mathbf{z}}$ is a vector of the standard spin-1 matrices

$$F^x = \begin{pmatrix} 0 & \eta & 0 \\ \eta & 0 & \eta \\ 0 & \eta & 0 \end{pmatrix}, \; F^y = i \begin{pmatrix} 0 & -\eta & 0 \\ \eta & 0 & -\eta \\ 0 & \eta & 0 \end{pmatrix}, \; F^z = \begin{pmatrix} 1 & 0 & 0 \\ 0 & 0 & 0 \\ 0 & 0 & -1 \end{pmatrix}, \tag{2.3}$$

where $\eta = 1/\sqrt{2}$. In Eq. (2.1) and what follows, the spin indices take the values $j, j', k, k' \in \{1, 0, -1\}$ and summation over repeated indices is assumed.

The coupling constants g_n and g_s appearing in Eq. (2.1) measure the strengths of the local density–density and spin–spin interactions, respectively. They are related to the s-wave scattering lengths a_0 and a_2 into spin channels with total spin 0 and $2\hbar$ through $g_\mathrm{n} = 4\pi\hbar^2\left(a_0 + 2a_2\right)/3m$ and $g_\mathrm{s} = 4\pi\hbar^2\left(a_2 - a_0\right)/3m$. The spin–spin interaction is referred to as ferromagnetic if $g_\mathrm{s} < 0$ and antiferromagnetic if $g_\mathrm{s} > 0$. Spinor condensates of ^{87}Rb are examples of the ferromagnetic case, whereas condensates of ^{23}Na have antiferromagnetic coupling.

In the Heisenberg picture, the quantum field operator $\hat{\psi}_j(\mathbf{r},t)$ evolves in time according to the Heisenberg equation of motion,

$$i\hbar\partial_t \hat{\psi}_j(\mathbf{r},t) = \left[\hat{\psi}_j(\mathbf{r},t), \hat{K}\right]. \tag{2.4}$$

By inserting the Hamiltonian (2.1) into Eq. (2.4) and using the canonical commutation relations

$$[\hat{\psi}_j(\mathbf{r},t), \hat{\psi}_k^\dagger(\mathbf{r}',t)] = \delta_{jk}\delta(\mathbf{r}-\mathbf{r}'), \quad [\hat{\psi}_j(\mathbf{r},t), \hat{\psi}_k(\mathbf{r}',t)] = 0, \tag{2.5}$$

we obtain

$$i\hbar\partial_t \hat{\psi}_j = \mathcal{H}_{jk}\hat{\psi}_k - \mu\hat{\psi}_j + g_\mathrm{n}\hat{\psi}_{j'}^\dagger\hat{\psi}_{j'}\hat{\psi}_j + g_\mathrm{s}\hat{\psi}_{j'}^\dagger \mathbf{F}_{j'k'}\hat{\psi}_{k'} \cdot \mathbf{F}_{jk}\hat{\psi}_k. \tag{2.6}$$

2.2 Definition of Bose–Einstein condensation

The onset of Bose–Einstein condensation is associated with the formation of off-diagonal long-range order in the system. A convenient way to characterize the condensation phenomenon and the existence of off-diagonal long-range order is provided by the Penrose–Onsager criterion [90], which relates these concepts to the single-particle density matrix ρ_1 defined as

$$\rho_1(j\mathbf{r}, j'\mathbf{r}'; t) = \langle \hat{\psi}^\dagger_{j'}(\mathbf{r}', t)\hat{\psi}_j(\mathbf{r}, t)\rangle. \tag{2.7}$$

Since $\rho_1(j\mathbf{r}, j'\mathbf{r}'; t)$ is an Hermitian matrix, it can be diagonalized in terms of single-particle eigenfunctions with real eigenvalues. According to the Penrose–Onsager criterion, a conventional Bose–Einstein condensate exists if ρ_1 has exactly one eigenvalue, N_0, that is of the order of the total number of particles, N, and the rest of the eigenvalues are much smaller than N. Furthermore, we define the condensate order parameter $\Psi = (\Psi_j) = (\Psi_{+1}, \Psi_0, \Psi_{-1})$ as the spinor-valued eigenfunction that corresponds to the eigenvalue N_0,

$$\int \mathrm{d}^3 r' \rho_1(j\mathbf{r}, j'\mathbf{r}'; t)\Psi_{j'}(\mathbf{r}', t) = N_0\Psi_j(\mathbf{r}, t), \tag{2.8}$$

and that is normalized such that $\int \mathrm{d}^3 r \Psi^*_j(\mathbf{r}, t)\Psi_j(\mathbf{r}, t) = N_0$. The ratio N_0/N is referred to as the condensate fraction.

2.3 Gross–Pitaevskii equation

In order to develop a mean-field theory for the dilute BECs, let us consider a system which has condensed according to the Penrose–Onsager criterion. Using the order-parameter field given by Eq. (2.8), we define the bosonic field $\hat{\chi}(\mathbf{r}, t) := \hat{\psi}(\mathbf{r}, t) - \Psi(\mathbf{r}, t)$, which allows us to decompose the quantum field operator as

$$\hat{\psi}_j(\mathbf{r}, t) = \Psi_j(\mathbf{r}, t) + \hat{\chi}_j(\mathbf{r}, t). \tag{2.9}$$

The order parameter Ψ describes the atoms in the coherent condensate, whereas the fluctuation operator $\hat{\chi}$ characterizes the noncondensed, or thermal, component of the gas.

In this dissertation, we will exclusively work in the limit of zero temperature. In such a setting, the fluctuation operator $\hat{\chi}$ is assumed to yield only a small correction to the overall state of the system, and the theory is developed as a perturbation expansion in the powers of $\hat{\chi}$. To this end,

we insert the decomposition in Eq. (2.9) into Eq. (2.6) and collect terms in orders of $\hat{\chi}$, yielding the zeroth-order equation,

$$i\hbar\partial_t\Psi_j = \left(\mathcal{H}_{jk} - \mu\delta_{jk} + g_{\rm n}\Psi^*_{j'}\Psi_{j'}\delta_{jk} + g_{\rm s}\Psi^*_{j'}\mathbf{F}_{j'k'}\Psi_{k'}\mathbf{F}_{jk}\right)\Psi_k, \tag{2.10}$$

which is the celebrated Gross–Pitaevskii (GP) equation [91–93] for spin-1 BECs, and the first-order equation

$$i\hbar\partial_t\hat{\chi}_j(\mathbf{r},t) = \left(\mathcal{H}_{jk} - \mu\delta_{jk} + \mathcal{C}_{jk}\right)\hat{\chi}_k(\mathbf{r},t) + \mathcal{B}_{jk}\hat{\chi}^\dagger_k(\mathbf{r},t), \tag{2.11}$$

where the self-energies are given by

$$\mathcal{B}_{jk} = g_{\rm n}\Psi_j\Psi_k + g_{\rm s}\mathbf{F}_{jj'}\cdot\mathbf{F}_{kk'}\Psi_{j'}\Psi_{k'}, \tag{2.12}$$

$$\begin{aligned}\mathcal{C}_{jk} = {} & g_{\rm n}\left(\Psi^*_{j'}\Psi_{j'}\delta_{jk} + \Psi_j\Psi^*_k\right) \\ & + g_{\rm s}\Big(\mathbf{F}_{jk}\cdot\mathbf{F}_{j'k'} + \mathbf{F}_{jk'}\cdot\mathbf{F}_{j'k}\Big)\Psi^*_{j'}\Psi_{k'}.\end{aligned} \tag{2.13}$$

The GP equation (2.10) forms the backbone of the mean-field analysis used in this dissertation. To solve Eq. (2.10) numerically, we discretize it on a uniform grid using finite-difference methods and compute the time evolution of $\Psi(\mathbf{r},t)$ with a split-operator approach [94, 95]. Often, we are interested in the stationary states of the condensate that satisfy the time-independent GP equation,

$$\left(\mathcal{H}_{jk} - \mu\delta_{jk} + g_{\rm n}\Psi^*_{j'}\Psi_{j'}\delta_{jk} + g_{\rm s}\Psi^*_{j'}\mathbf{F}_{j'k'}\Psi_{k'}\cdot\mathbf{F}_{jk}\right)\Psi_k(\mathbf{r}) = 0. \tag{2.14}$$

Its numerical solutions are obtained with the technique of successive over-relaxation [94].

2.4 Elementary excitations

In this section, we study the low-energy elementary excitations of the BEC in the zero-temperature limit. Elementary excitations are closely related to the collective oscillations of the system and characterize its response to small external perturbations, often enabling a lucid comparison between theory and experiments. The theoretical formalism for trapped spin-1 BECs [96, 97] is based on the framework established by Bogoliubov in 1947 for a uniform gas of interacting bosons [98]. The basic idea is to expand the Hamiltonian (2.1) in powers of $\hat{\chi}$ about a stationary state of the condensate and diagonalize the resulting second-order term by a canonical operator transformation.

To study the small-amplitude oscillations in the vicinity of a given stationary state $\Psi(\mathbf{r})$, we write the field operator in the form $\hat{\psi}(\mathbf{r},t) = \Psi(\mathbf{r}) +$

$\hat{\chi}(\mathbf{r},t)$, where $\Psi(\mathbf{r})$ satisfies Eq. (2.14). Equation (2.11) for the noncondensate operator $\hat{\chi}$ is then solved by introducing the Bogoliubov transformation

$$\hat{\chi}_j(\mathbf{r},t) = \sum_q \left[u_{q,j}(\mathbf{r}) e^{-i\omega_q t} \hat{b}_q + v^*_{q,j}(\mathbf{r}) e^{i\omega^*_q t} \hat{b}^\dagger_q \right], \tag{2.15}$$

where $\hat{b}_q$ and $\hat{b}^\dagger_q$ are the annihilation and creation operators for bosonic quasiparticles with energy $\hbar\omega_q$. We require the transformation to be canonical, which implies that the quasiparticle amplitudes (u_q, v_q) must satisfy the orthonormality condition

$$\int \mathrm{d}^3 r \left[u^*_{q,j}(\mathbf{r}) u_{q',j}(\mathbf{r}) - v^*_{q,j}(\mathbf{r}) v_{q',j}(\mathbf{r}) \right] = \delta_{qq'}. \tag{2.16}$$

Inserting Eq. (2.15) into Eq. (2.11) yields the Bogoliubov equation for the elementary excitations

$$\begin{pmatrix} \mathcal{A}_{jk} & \mathcal{B}_{jk} \\ -\mathcal{B}^*_{jk} & -\mathcal{A}^*_{jk} \end{pmatrix} \begin{pmatrix} u_{q,k}(\mathbf{r}) \\ v_{q,k}(\mathbf{r}) \end{pmatrix} = \hbar\omega_q \begin{pmatrix} u_{q,j}(\mathbf{r}) \\ v_{q,j}(\mathbf{r}) \end{pmatrix}, \tag{2.17}$$

where $\mathcal{A}_{jk} = \mathcal{H}_{jk} - \mu\delta_{jk} + \mathcal{C}_{jk}$.

It is noteworthy that the Bogoliubov matrix in Eq. (2.17) is generally not Hermitian, which permits the existence of eigensolutions with nonreal eigenfrequencies ω_q. Such excitation modes are referred to as *complex modes*. However, the complex modes are not proper quasiparticle solutions in the sense that they do not satisfy the orthonormality condition of Eq. (2.16) [99,100]. Thus, the existence of complex modes indicates the failure of the usual Bogoliubov transformation [101] and special care must be taken in quantizing them [31,102].

When the Bogoliubov spectrum is used to expand the grand-canonical Hamiltonian (2.1), the resulting diagonalized form shows that the creation of a quasiparticle corresponding to a real eigenfrequency ω_q increases the energy of the state by $\hbar\omega_q$, whereas the energy cost of populating complex modes vanishes. Therefore, the complex modes can become excited even when there is no mechanism for energy exchange between the system and the environment.

Stability criteria

The Bogoliubov excitation spectrum can be used to classify the stability of the condensate states. By definition, a physical system is *locally energetically stable* if its state is a local minimum of the free energy functional

under the relevant constraints.[2] In terms of the excitation spectrum, local energetical stability is equivalent to all excitation energies $\hbar\omega_q$ being positive. This means that the coherent part of the gas cannot lower its energy by exciting quasiparticles. The existence of an excitation with negative energy renders the stationary state *locally energetically unstable*, indicating that it does not correspond to a local minimum of the mean-field energy. By populating these negative-energy modes, the coherent condensate is able to dissipate energy to its environment. Since the dissipative environment consists mainly of the thermal gas, energetically unstable states can still be quite long-lived if the temperature—and hence the density of the thermal gas—is kept sufficiently low.

Another important stability concept is *dynamical stability*, or Lyapunov stability [103]. In Publications I–III, dynamical stability is studied in the context of multiply quantized vortices. Dynamical stability is a weaker condition than energetical one, since energetically stable systems are always dynamically stable [104]. Essentially, a system is dynamically stable if small perturbations to its state cause only small deviations in its time development. Dynamical stability is intimately related to the existence of complex modes: As can be observed from Eq. (2.15), the amplitude of a small perturbation associated with the excitation of a complex mode initially evolves exponentially in time. Consequently, stationary states that support complex modes are dynamically unstable. On the other hand, if all excitation energies of a stationary state are real, the state is dynamically stable. Dynamical instabilities are particularly relevant for the BEC experiments, since their effect cannot be disposed of by reducing temperature.

[2] If this minimum is absolute, the state is called *globally energetically stable*, or thermodynamically stable, and it is the ground state of the system.

3. Creation and Properties of Multiquantum Vortices in Dilute Bose–Einstein Condensates

This chapter is devoted to quantized vortices which manifest the quantum phase coherence of the BEC and characterize its response to external rotation. The concept of a quantized vortex is introduced in Sec. 3.1, and a topological method to create them is described in Secs. 3.2 and 3.3. This method also makes it possible to create vortices with multiple quanta; the properties of such vortices, in conjunction with the results of Publications I–III, are discussed in Secs. 3.4–3.6.

3.1 Quantized vortices in Bose–Einstein condensates

The idea of quantized vortices was originally put forward by Onsager [105] and Feynman [106] when considering the hydrodynamics of superfluid helium. In nature, whirlwinds of various kinds, such as tornadoes, dust devils, and waterspouts, serve as classical analogs to the vortices in the quantum realm.

By starting from the expression for the particle current density,

$$\mathbf{j}(\mathbf{r}) = n(\mathbf{r})\mathbf{v}(\mathbf{r}) = \frac{\hbar}{2im}\left(\Psi_j^*\nabla\Psi_j - \Psi_j\nabla\Psi_j^*\right), \tag{3.1}$$

and factorizing the order parameter into the particle density n and a unit-normalized spinor ζ as $\Psi(\mathbf{r}) = \sqrt{n(\mathbf{r})}\zeta(\mathbf{r})$, we can write the velocity field of the condensate as [89, 107]

$$\mathbf{v}(\mathbf{r}) = \frac{\hbar}{im}\zeta_j^*(\mathbf{r})\nabla\zeta_j(\mathbf{r}). \tag{3.2}$$

The line integral of $\mathbf{v}$ around a closed loop γ defines the circulation

$$\Gamma = \oint_\gamma \mathrm{d}\mathbf{l}\cdot\mathbf{v}(\mathbf{r}). \tag{3.3}$$

For clarity, let us first consider a scalar BEC with a single-component order parameter, say, $\Psi_j = \Psi_1\delta_{j,1}$. In this case, the unit spinor ζ can be

written simply as $\zeta_j(\mathbf{r}) = e^{iS(\mathbf{r})}\delta_{j,1}$, where $S(\mathbf{r})$ is a real-valued phase field. Consequently, the velocity $\mathbf{v}$ in Eq. (3.2) is found to be proportional to the gradient of the phase, $\mathbf{v} = \hbar\nabla S(\mathbf{r})/m$. It immediately follows from this expression that the velocity field must be irrotational, i.e., $\nabla \times \mathbf{v} = \mathbf{0}$, unless there is a singularity in the phase S. Moreover, since the order parameter must be continuous, its phase S may only change through a multiple of 2π along a closed path. Hence, Eq. (3.3) implies that the circulation in the scalar BEC is quantized in units of h/m,

$$\Gamma = \frac{\hbar}{m} 2\pi\kappa, \tag{3.4}$$

where κ is an integer winding number. If $\kappa \neq 0$, the path γ encircles a *vortex line*—a one-dimensional singularity in the phase field S. The particle density must vanish at the singularity, giving rise to the *core* of the vortex. A vortex line whose winding number satisfies $|\kappa| \geq 2$ is referred to as a *multiquantum vortex* and typically constitutes an energetically unstable state. Such vortices are discussed in Secs. 3.2–3.6. Vortices having $\kappa < 0$ in the chosen coordinate system are called *antivortices*.

Quantized vortices are conventionally interpreted as the signature of superfluidity and quantum phase coherence. Vortices may also be considered as the quantized response of the irrotational condensate to a sufficiently strong external rotation. Indeed, if one tries to rotate a cylindrically symmetric BEC about its axis of symmetry, it remains at rest until the first critical rotation frequency Ω_{c1} is reached, beyond which it becomes energetically favorable for the condensate to nucleate a quantized vortex. Rotation at a frequency $\Omega \gg \Omega_{\mathrm{c1}}$ will result in the formation of several vortices typically arranged into a triangular, so-called Abrikosov lattice [108]. In experiments with atomic BECs, Abrikosov lattices consisting of up to over a hundred vortices have been created, e.g., by stirring the condensate with a focused laser beam [109–112]. Vortex lattices in a system of two interacting condensates are studied in detail in Sec. 4.2.

In the scalar BEC, the circulation Γ defined in Eq. (3.3) is always quantized, and the vortices are of the singular, mass-current-carrying type discussed above. In spinor BECs, on the contrary, Γ is not in general quantized, and the multicomponent nature of the order parameter allows for a richer variety of vortices. Here, we consider only the ferromagnetically coupled spin-1 BEC ($g_{\mathrm{s}} < 0$) due to its relevance to Publications III, VI and VII. Its order-parameter space in the ferromagnetic phase has a group structure corresponding to $\mathrm{SO}(3)$, the group of three-dimensional rotations [89]. The antiferromagnetically coupled spin-1 BEC ($g_{\mathrm{s}} > 0$) gives

rise to the order-parameter space $\left[\mathrm{U}(1) \times S^2\right]/\mathbb{Z}_2$, and it also supports a wide selection of topological defects including skyrmions [65], monopoles [66], and half-quantum vortices [60–64].

In the ferromagnetically coupled spin-1 BEC, the local magnetization $\mathbf{M}(\mathbf{r}) = \Psi_j^*(\mathbf{r})\mathbf{F}_{jk}\Psi_k(\mathbf{r})$ tends to be maximized. Since $\mathbf{M}(\mathbf{r})$ can have spatial dependence, the system can exhibit both mass and spin currents, and consequently two kinds of circulations exist. The vortices encountered in this dissertation can be characterized with two winding numbers κ_m and κ_s corresponding to the mass and the spin circulation, respectively.

A vortex carrying both mass and spin currents with equal or opposite winding numbers, $|\kappa_\mathrm{m}| = |\kappa_\mathrm{s}|$, is referred to as a *Mermin–Ho vortex* [97, 113]. The Mermin–Ho vortex is an example of a coreless vortex [114, 115] that can be continuously changed into a uniform spin texture. Its core exhibits a finite particle density and a nonvanishing magnetization.

Another type of vortex prominent in ferromagnetically coupled spin-1 BECs is the *polar-core vortex* [96, 97, 116–120], which carries only spin current ($\kappa_\mathrm{s} \neq 0$, $\kappa_\mathrm{m} = 0$) and has a nonmagnetized core. The particle density, on the other hand, does not vanish at the core, but instead the region is occupied by antiferromagnetically ordered condensate matter. Thus, the polar-core vortex constitutes an interesting example of the coexistence of competing magnetic phases in spinor condensates. Except for the filled polar core, these vortices are analogous to the so-called disgyrations found in the fermionic superfluid ^{3}He-A, which is also characterized by the order-parameter space $\mathrm{SO}(3)$ in its dipole-locked phase [121, 122].

3.2 Topological creation of multiquantum vortices

The first multiply quantized vortices were created in 2002 by using the topological phase engineering method [71] that was originally proposed by Nakahara *et al.* [123] and subsequently studied in Refs. [124–130]. In this technique, the phase winding associated with a multiquantum vortex is obtained by rotating the spins of the condensate atoms about an axis that depends on the location of a particular atom. Recently, it has also been theoretically demonstrated that topological phase engineering can be used to create a Dirac monopole in a spinor BEC [69].

In accordance with the original proposal and the experiment [71], we consider a spin-F BEC confined in a Ioffe–Pritchard (IP) trap [131]. This type of magnetic trap is formed by four Ioffe bars aligned parallel to the

z axis, each carrying a current of equal magnitude and providing confinement in the xy plane, and two circular coils generating confinement in the z direction. In the plane $z = 0$, the IP field can be written as a sum of a quadrupole field $\mathbf{B}_{\rm q}$ and a uniform axial bias field $\mathbf{B}_z$,

$$\mathbf{B}(r, \phi, z = 0, t) = \mathbf{B}_{\rm q}(r, \phi) + \mathbf{B}_z(t) = B'_{\rm q} r \left(\cos\phi \hat{\mathbf{x}} - \sin\phi \hat{\mathbf{y}}\right) + B_z(t)\hat{\mathbf{z}}, \quad (3.5)$$

where $B'_{\rm q}$ is the radial gradient of the quadrupole field and (r, ϕ, z) denote the cylindrical coordinates. The IP trap provides confinement for the so-called weak-field seeking states of the spin-F BEC, which correspond to the eigenvalues $m_z g_F \mu_{\rm B} |\mathbf{B}|$, $m_z \in \{1, \ldots, F\}$, of the linear Zeeman Hamiltonian[1] $\mathcal{H}_{\rm Z} = g_F \mu_{\rm B} \mathbf{B} \cdot \mathbf{F}$. For concreteness, we have assumed that $g_F > 0$.

To topologically imprint a multiquantum vortex in a IP trap, the axial bias field $B_z(t)$ is initially set strong enough to render the BEC essentially spin-polarized along the z axis, with all atomic spins residing in the eigenstate $|F, m_z\rangle$ of $\mathcal{H}_{\rm Z}$. The bias field $B_z(t)$ is then reversed adiabatically, i.e., sufficiently slowly such that the individual spins follow the local magnetic field and the system remains in the instantaneous eigenstate of $\mathcal{H}_{\rm Z}$. Since spins at different locations rotate about different axes, the order parameter acquires a spatially dependent $\mathrm{U}(1)$ phase factor that is associated with the presence of a multiply quantized vortex.

In order to describe the process mathematically, let us write the unit vector of the magnetic field as $\hat{\mathbf{b}} = \sin\beta\cos\alpha\,\hat{\mathbf{x}} + \sin\beta\sin\alpha\,\hat{\mathbf{y}} + \cos\beta\,\hat{\mathbf{z}}$, where (α, β) form the standard parametrization of the unit sphere. The eigenstates of $\mathcal{H}_{\rm Z}$ can then be written in the general form $\mathcal{R}\left(\hat{\mathbf{n}}(\alpha); \beta\right)|F, m_z\rangle$, where the unitary operator $\mathcal{R}\left(\hat{\mathbf{n}}(\alpha); \beta\right) = \exp\left[-i\beta\hat{\mathbf{n}}(\alpha)\cdot\mathbf{F}\right]$ rotates the local spin by an angle β about the unit vector $\hat{\mathbf{n}}(\alpha) = -\sin\alpha\,\hat{\mathbf{x}} + \cos\alpha\,\hat{\mathbf{y}}$ perpendicular to $\hat{\mathbf{b}}$. For the IP field, Eq. (3.5) yields $\alpha = -\phi$ and $\beta = \tan^{-1}\left[B_q r / B_z(t)\right]$. Assuming that the initial and final values of the bias field satisfy $B_z(0) \approx -B_z(T) \gg B'_q R$, where R is the condensate radius and T is the time duration of the reversal, the field reversal rotates the spins essentially by $\beta = \pi$ about the normal vector of the quadrupole field, $\hat{\mathbf{n}}_{\rm q}\left(\phi\right) = \sin\phi\,\hat{\mathbf{x}} + \cos\phi\,\hat{\mathbf{y}}$. Thus, the final state is given by

$$\mathcal{R}\left(\hat{\mathbf{n}}_{\rm q}(\phi); \pi\right)|F, m_z\rangle = (-1)^{F+m_z} e^{-2im_z\phi}|F, -m_z\rangle, \quad (3.6)$$

corresponding to a vortex with a quantum number $\kappa = -2m_z$.

In the experiment [71], condensates of ^{23}Na were prepared in the hyperfine states $|F = 1, m_z = -1\rangle$ and $|F = 2, m_z = 2\rangle$ in a IP trap. The

[1] In this section and the next, we assume the spin-F operator $\mathbf{F}$ to be given in the $(2F+1)$-dimensional irreducible representation of $\mathrm{SO}(3)$ or $\mathrm{SU}(2)$.

vortices were created by reversing B_z linearly in time, and they could be removed by reversing the bias field back to its original direction. The orbital angular momentum per particle was measured using surface-wave spectroscopy [132, 133], yielding $\langle \hat{L}_z \rangle / N \approx 2\hbar$ for the state $|1, -1\rangle$ and $\langle \hat{L}_z \rangle / N \approx -4\hbar$ for the state $|2, 2\rangle$, which correspond to a two-quantum and a four-quantum vortex, respectively.

3.3 Vortex pump for Bose–Einstein condensates

In a IP trap, the topological phase engineering technique enables the creation of a $2F$-quantum vortex in a BEC with total hyperfine spin F. As discussed above, the phase winding of the vortex is created by an azimuthally dependent reversal of the external magnetic field. Reversing the field back to its original configuration would cause the vortex to unwind itself, and the resulting state would again have no orbital angular momentum. In principle, vortices with large quantum numbers could be created in the IP trap by using atoms with larger values of the hyperfine spin F. However, this approach quickly becomes impractical, since manipulation of atoms with large F is experimentally very challenging.

On the other hand, if higher-order magnetic fields such as the hexapole field are employed in place of the quadrupole field $\mathbf{B}_\mathrm{q}$, it becomes possible to create more than $2F\hbar$ of orbital angular momentum per particle with a single bias field reversal. Indeed, this is the essential observation that forms the basis for the *vortex pump* introduced by Möttönen *et al.* [73]: Initially, $B_z < 0$ and the condensate is prepared in the spin state $|F, m_z = -F\rangle$ without a vortex. By using the hexapole field

$$\mathbf{B}_\mathrm{h}(r, \phi) = B_h' r \left[\cos(2\phi)\, \hat{\mathbf{x}} - \sin(2\phi)\, \hat{\mathbf{y}}\right] \tag{3.7}$$

during the first bias field reversal, a $4F$-quantum vortex is produced. In terms of the spin rotations discussed above, this is expressed as the operation $\mathcal{R}(\hat{\mathbf{n}}_\mathrm{h}(\phi); -\pi)|F, -F\rangle = e^{i4F\phi}|F, F\rangle$, where the normal vector of the hexapole field is given by $\hat{\mathbf{n}}_\mathrm{h}(\phi) = \sin(2\phi)\, \hat{\mathbf{x}} + \cos(2\phi)\, \hat{\mathbf{y}}$. Then, switching $\mathbf{B}_\mathrm{h}$ to $\mathbf{B}_\mathrm{q}$ and reversing the bias field $\mathbf{B}_z$ back to its original value, only $2F\hbar$ of orbital angular momentum per particle is lost, and the final spin state becomes

$$\mathcal{R}(\hat{\mathbf{n}}_\mathrm{q}(\phi); \pi)\mathcal{R}(\hat{\mathbf{n}}_\mathrm{h}(\phi); -\pi)|F, -F\rangle = e^{i2F\phi}|F, -F\rangle. \tag{3.8}$$

Hence the final state has accumulated $2F\hbar$ of orbital angular momentum

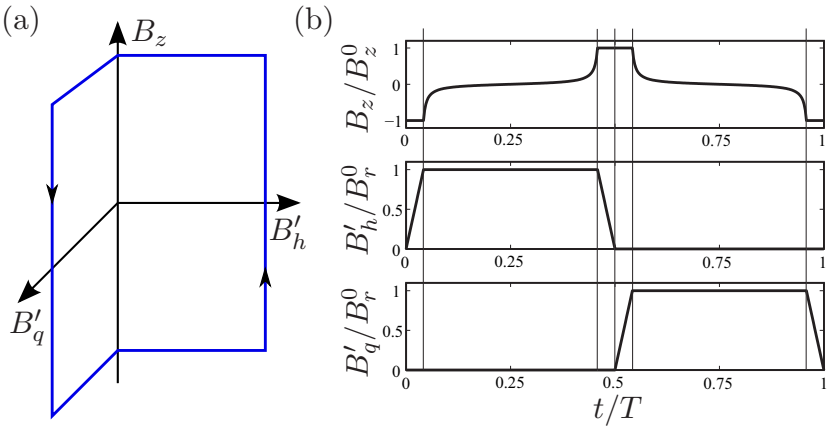

Figure 3.1. (a) Control cycle of the vortex pump in the magnetic-field parameter space. Here, B'_q and B'_h are the radial derivatives of the quadrupole and hexapole field magnitudes, and B_z is the uniform axial bias field. (b) The control parameters as a function of time for the pumping cycle used in Publication III. The common maximum value of B'_q and B'_h is denoted by B_r^0, and T is the duration of the cycle. The time dependence of B_z is such that spins at a fixed distance from the z axis are reversed with constant speed.

per particle. This process can then be repeated, and each cycle increases the vorticity of the condensate by $2F$ quanta.

Figure 3.1 illustrates a possible pumping cycle, which is identical to the one used in Ref. [73] and is presented in more detail in Publication III. The control parameters consist of the axial bias field $B_z(t)$ and the radial gradients of the quadrupole and hexapole fields, $B'_{\rm q}(t)$ and $B'_{\rm h}(t)$. The control cycle can be operated both fully adiabatically and partly nonadiabatically [73]. In the former case, an additional optical potential is needed to confine the condensate during moments when both multipole fields vanish. Furthermore, in order to stabilize the vortex and prevent it from splitting, an optical plug potential can be employed; in Publication III, this approach is used to demonstrate the adiabatic creation of an unsplit 20-quantum vortex. The partly nonadiabatic operation, on the other hand, can be carried out without any optical potentials, but with the cost of losing a part of the atoms from the trap. Later, Xu *et al.* [134, 135] have investigated alternative pumping cycles utilizing magnetic-field setups different from the original proposal.

The vortex pump can be interpreted in terms of the geometric Berry phase accumulated by the individual spins of the condensed atoms [73]. According to the result by Berry [136], an adiabatically and cyclically turned spin acquires a geometric phase equal to $-m_z\Omega_{\rm s}$, where $\Omega_{\rm s}$ is the solid angle subtended by the path of the spin with the initial state $|F, m_z\rangle$.

In the case of the pumping cycle of Fig. 3.1, Ω_{s} equals twice the angle between the normal vectors $\hat{\mathbf{n}}_{\mathrm{q}}$ and $\hat{\mathbf{n}}_{\mathrm{h}}$. For $m_z = -F$, this yields a local Berry phase of $2F\phi$, consistent with the accumulation of $2F$ quanta of vorticity per cycle. [2]

3.4 Core sizes and dynamical instabilities of giant vortices

In Publication I, the vortex core sizes and dynamical instabilities of axisymmetric giant vortex states are studied in nonrotated BECs as functions of the vorticity quantum number κ and the interaction strength g. The investigation is motivated by the following considerations:

1. Earlier studies on the stability of multiquantum vortices have focused on the regime $\kappa \leq 5$ [48,52–55,137], most likely because previously there has been no realizable method to controllably create isolated vortices with large quantum numbers. However, the recently introduced vortex pump provides such an opportunity.

2. We aim to determine how large winding numbers the pump can reach for a single vortex. In principle, vortex pumping enables a controlled, adiabatic production of vortices with arbitrarily large κ. However, in real experiments κ will be limited by the stability properties of the vortex states. In particular, the existence of dynamical instabilities (Sec. 2.4) renders a giant vortex prone to splitting into single-quantum vortices, and the frequencies of these instabilities can be used to approximate its lifetime. On the other hand, the size of the vortex core is known to increase with increasing κ. As explained in Publication I, this enables one to speed up the pumping cycle without compromising adiabaticity as more vorticity accumulates in the BEC. Consequently, the interplay between the core size and the lifetime of the vortex as a function of κ ultimately determines the maximum winding number reachable with the pump.

We search for spin-polarized solutions to the time-independent GP equa-

[2] A similar kind of reasoning can also be used to explain the vortex creation method discussed in Sec. 3.2 by considering the geometric phase difference between two spins located at different values of the azimuthal coordinate ϕ [125, 129].

tion, Eq. (2.14), that describe stationary axisymmetric κ-quantum vortices in pancake-shaped condensates.[3] Such states can be written as

$$\Psi_j(r,\phi,z) = f(r)e^{i\kappa\phi}\zeta_0(z)\delta_{j,1}, \tag{3.9}$$

where $\zeta_0(z) = \exp\left(-z^2/2a_z^2\right)/\sqrt[4]{\pi a_z^2}$, $a_z = \sqrt{\hbar/m\omega_z}$, and $f(r)$ is a real-valued function to be determined. For stationary states of this form, the quasiparticle amplitudes can be expressed as

$$\begin{aligned} u_{q,j}(r,\phi,z) &= u_q(r)\zeta_0(z)e^{i(l_q+\kappa)\phi}\delta_{j,1}, \\ v_{q,j}(r,\phi,z) &= v_q(r)\zeta_0(z)e^{i(l_q-\kappa)\phi}\delta_{j,1}, \end{aligned} \tag{3.10}$$

where l_q is an integer that determines the orbital angular momentum of the excitation with respect to the condensate. The stationary states and the corresponding Bogoliubov excitation spectra are solved for the parameter ranges $0 \le \kappa \le 100$ and $0 \le \tilde{g} \le 10^4$, where the dimensionless interaction strength is $\tilde{g} = \sqrt{8\pi}Na_2/a_z$. In typical experiments, $10^2 \le \tilde{g} \le 10^6$.

The main results of Publication I are presented in Fig. 3.2, where the core sizes and the dominant dynamical instabilities of the giant vortices are plotted as functions of the winding number κ. The vortex core radius r_c is found to be a strictly increasing function of κ with the asymptotic behavior $\tilde{r}_\mathrm{c} \propto \sqrt{\kappa}$ for large κ [Fig. 3.2(a)]. Publication I also presents an analytical estimate for r_c that is in good agreement with the numerically obtained radius. On the other hand, the maximum strength of the dynamical instability of a κ-quantum vortex turns out to increase slowly with κ or even to saturate to a relatively low value [Fig. 3.2(b)].

Publication I provides the first systematic study of the instabilities of quantized vortices with extremely large winding numbers κ. From the point of view of the vortex pump (Sec. 3.3), the obtained results are encouraging. Qualitatively, the efficiency of the pump in producing vortices with large winding numbers is described by the ratio τ_sp/T, where τ_sp is a characteristic time scale for vortex splitting and T is the duration of the pumping cycle. Since the radius of the vortex core increases monotonously with the winding number, it should be possible to gradually decrease T and still retain the adiabaticity of the process. On the other hand, the splitting times $\tau_\mathrm{sp} \propto 1/\max_q |\mathrm{Im}\,(\omega_q)|$ decrease only slowly with κ for large vorticities. Consequently, the ratio τ_sp/T can—at least ideally—be

[3] BECs in traps that satisfy $\omega_z \gg \omega_r$ are called pancake shaped, whereas traps with $\omega_z \ll \omega_r$ produce cigar-shaped condensates.

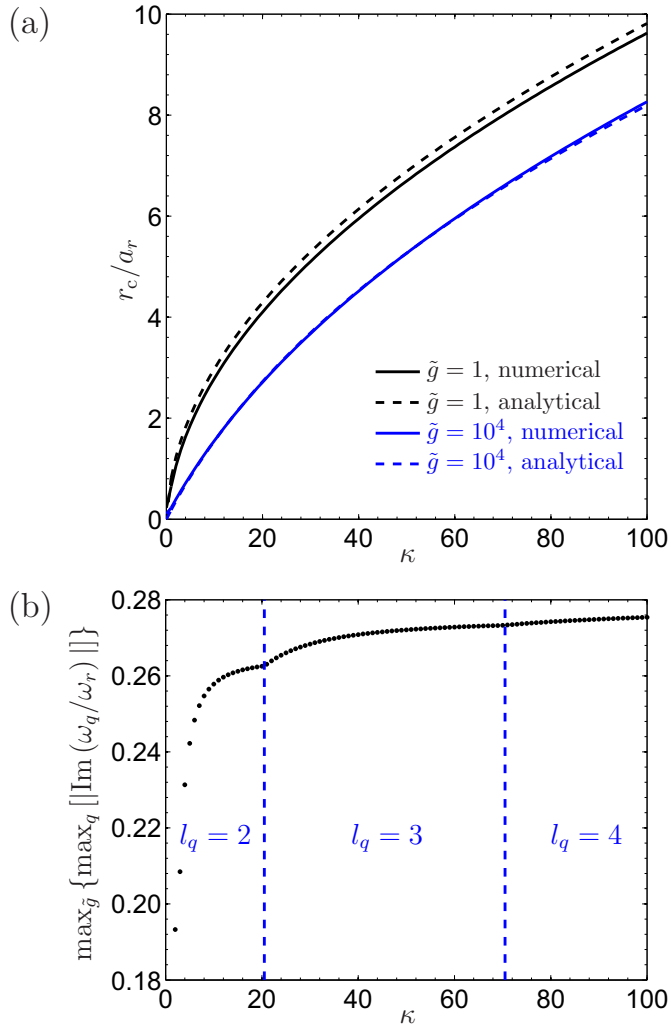

Figure 3.2. (a) Radius r_c of the vortex core as a function of the winding number κ for $\tilde{g} = 1$ and $\tilde{g} = 10^4$. (b) The maximum dynamical instability of a giant vortex state, $\max_{\tilde{g}} \{\max_q [|\mathrm{Im}(\omega_q/\omega_r)|]\}$, as a function of κ. This parameter is maximized over the interaction strength $\tilde{g}$ and thus depends only on κ. The dashed vertical lines indicate the points at which the angular-momentum quantum number l_q of the dominant complex mode changes.

increased after a sufficient amount of vorticity has accumulated into the condensate. Hence, our results suggest that giant vortices with very high winding numbers may be achieved by gradually increasing the operation frequency of the pump.

3.5 Splitting dynamics of giant vortices

Besides being generally energetically unstable, states with a multiquantum vortex are often also dynamically unstable in harmonic traps [48, 52–55]. Dynamical instability is a peculiar feature of nonlinear dynamics through which small perturbations of a stationary state can lead to large structural changes, even in the absence of dissipation (cf. Sec. 2.4). In the case of multiquantum vortices, the existence of dynamical instabilities indicates that the multiquantum vortex is unstable against splitting into single-quantum vortices. Experimentally, the splitting process has been investigated for two-quantum and four-quantum vortices, and they were observed to dissociate into a linear chain of single-quantum vortices [130, 138, 139], in accordance with theoretical predictions [140–142].

Motivated by the fact that the vortex pump opens the possibility of realizing stationary vortex states with very large winding numbers, we investigate in Publication II the splitting dynamics of multiquantum vortices for an unprecedently wide range of winding numbers, $2 \leq \kappa \leq 50$; in the previous studies, the focus has been on the regime $2 \leq \kappa \leq 5$. The splitting is studied in spin-polarized condensates both by directly computing the temporal evolution of the condensate from the time-dependent GP Eq. (2.10) and by solving the Bogoliubov excitation spectra to predict the essential features of the splitting process. We start from an initially stationary multiquantum vortex state and, to trigger the splitting, perturb it by adding either small-amplitude random noise or a complex-frequency Bogoliubov excitation to its order-parameter field.

Vortices with large winding numbers turn out to be dynamically unstable at nearly all values of the interaction strength $\tilde{g}$. When the dynamically unstable vortex states are perturbed with random noise, the vortex is found to dissociate through one of three possible splitting mechanisms, referred to as linear, threefold, and fourfold splitting. The results are summarized in Fig. 3.3(a), where the noise-induced splitting patterns are compared with the values of the quantum number l_q [Eq. (3.10)] of the dominant complex mode. Typically, the noise-induced splitting pat-

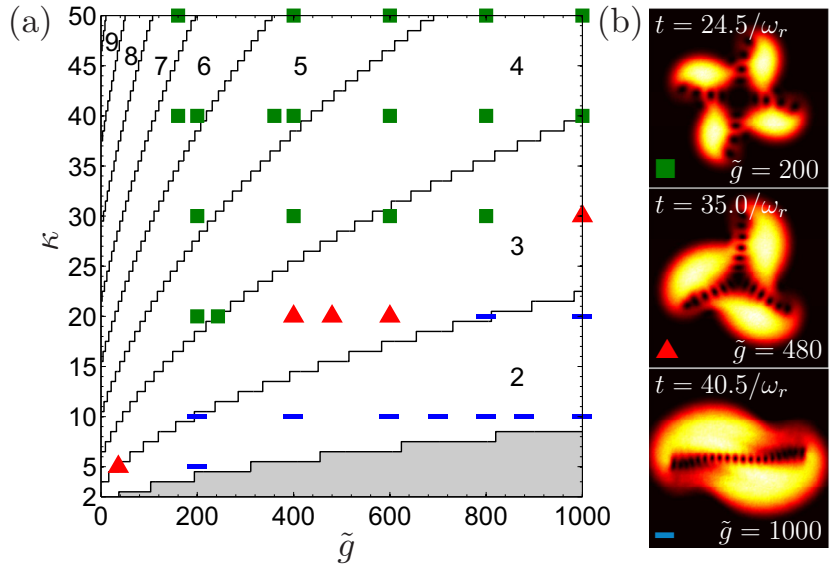

Figure 3.3. Noise-induced splitting of giant vortices. (a) The observed splitting patterns and dominant complex modes of stationary multiquantum vortices in the $(\tilde{g}, \kappa)$ plane. The lines separate regions where the angular-momentum quantum number l_q of the dominant complex mode is constant and has the value indicated. The shaded area corresponds to alternating values of l_q and regions of dynamical stability. The bars, triangles, and squares indicate splitting patterns with 2-, 3-, and 4-fold symmetries, respectively, resulting from the addition of small-amplitude random noise. (b) Density profiles obtained for $\kappa = 20$ and different values of $\tilde{g}$ illustrating the three types of splitting. The field of view in each panel is $18a_r \times 18a_r$, where $a_r = \sqrt{\hbar/m\omega_r}$ is the radial harmonic oscillator length.

tern is found to reflect the rotational symmetry of this excitation, which indicates that the splitting of the vortex can usually be ascribed to the dominant complex mode.

The three possible splitting patterns are exemplified for 20-quantum vortices in Fig. 3.3(b). The splitting proceeds through the creation of vortex sheets and results in separate, vortex-free domains of condensed atoms. We also find these splitting mechanisms to be robust against dissipation. Our results indicate that a giant vortex does not split by melting into a chaotic liquid of singly quantized vortices. Instead, the long-time dynamics preserves the rotational symmetry of the excitation mode responsible for the splitting. Therefore, the vortex pump may not be an efficient way to realize a strongly correlated vortex liquid phase [143] as envisioned in Ref. [73].

The novel vortex splitting patterns discovered in Publication II would enable a lucid comparison between theory and experiment. The splitting of the condensate into distinct fragments is detectable with current imaging techniques, and would allow for the clear identification of the angular-momentum quantum number l_q of the split-inducing excitation. Thus, the realization of an isolated giant vortex, e.g., with the vortex pump, and the consequent observation of its splitting would provide a means to directly relate the experimental data to discrete theoretical quantities.

3.6 Stabilization and pumping of giant vortices

In principle, the vortex pump (Sec. 3.3) enables a controlled production of vortices with arbitrarily large quantum numbers κ. However, as discussed above, vortices with large κ are dynamically unstable and prone to split into singly-quantized vortices, which poses a serious challenge to reaching high vorticities through adiabatic pumping. In Publication III, we address this issue by investigating how vortices with large κ can be made dynamically stable in nonrotated harmonically trapped BECs. As our method of choice, we study the effect of applying a repulsive Gaussian-shaped optical plug potential along the symmetry axis of the trap.

The plug is incorporated into the scalar GP mean-field model by augmenting the optical trap potential $V(\mathrm{r})$ in Eq. (2.2) with the Gaussian term

$$V_{\mathrm{plug}}(r) = Ae^{-r^2/d^2}, \tag{3.11}$$

where A denotes the amplitude of the plug and d is its beamwidth. This

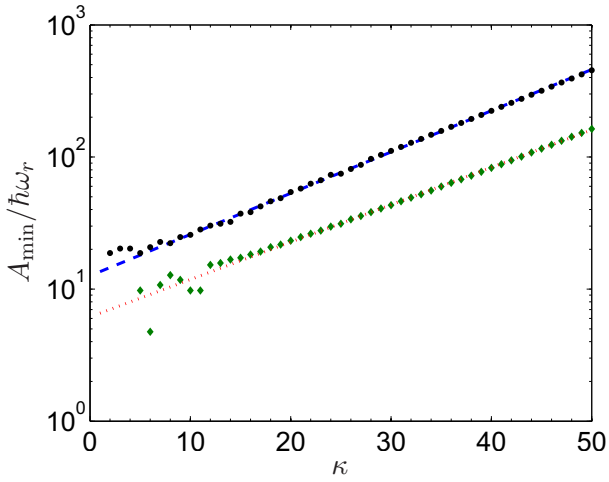

Figure 3.4. Minimum plug amplitude $A_{\min}$ required to stabilize vortices with a given winding number κ. The black dots indicate values that stabilize the vortices in the whole interval $0 \leq \tilde{g} \leq 2000$, and the dashed blue line is the least-squares fit $A_{\min} = 13\hbar\omega_r \exp(0.072\kappa)$. The green diamonds show the values that stabilize the vortex for fixed $\tilde{g} = 250$, and the dotted red line represents the fit $A_{\min} = 6.2\hbar\omega_r \exp(0.065\kappa)$. In both cases, the width of the plug is set to $d = 3a_r$.

type of potential can be realized in experiments by a tightly focused far-blue-detuned laser beam [17, 111, 112, 144–146]. In the vortex pump, the plug not only serves to stabilize the vortex but also prevents unwanted spin flips in the central region of the trap.

To study the vortex stabilization numerically, we solve the stationary GP equation and the Bogoliubov equations for different values of the winding number κ, interaction strength $\tilde{g}$, plug amplitude A, and beamwidth d, and determine the values of A and d that are sufficient to render the multiquantum vortices at given κ and $\tilde{g}$ dynamically stable. The results are shown in Fig. 3.4, where we plot, as a function of κ, the limiting plug amplitude $A_{\min}$ above which the κ-quantum vortex is dynamically stable for all values of $\tilde{g}$. The stabilizing amplitude $A_{\min}$ is found to increase exponentially with κ for sufficiently large winding numbers.[4] Importantly, the stabilizing values are small enough to be realizable with laser powers that are available for BEC experiments. Thus, these results suggest that achieving dynamical stability is feasible up to high quantum numbers.

In order to demonstrate the efficiency of the stabilization method, we

[4] If we fix the amplitude A and determine the smallest beamwidth, $d_{\min}$, that dynamically stabilizes the κ-quantum vortex for all $\tilde{g}$, we find that $d_{\min}$ increases as a square-root function of κ.

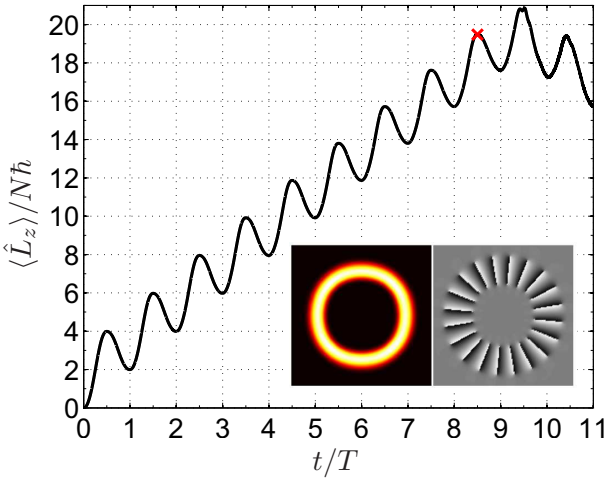

Figure 3.5. Orbital angular momentum of the condensate as a function of time during the vortex pump simulation of Publication III. The inset shows the particle density and phase of the 20-quantum vortex (field of view $18a_r \times 18a_r$) at the time instant $t = 8.5T$ marked with the red cross. Here, $T = 360/\omega_r$ is the duration of the pumping cycle. The coupling constants are given by $\tilde{g}_\mathrm{n} = \sqrt{8\pi} N \left(a_0 + 2a_2\right)/3a_z = 250$ and $g_\mathrm{s}/g_\mathrm{n} = -0.01$.

also show in Publication III that by utilizing a sufficiently strong plug potential, the vortex pump can be used to adiabatically create an unsplit giant vortex with a very large winding number. We consider a spin-1 BEC and compute the time evolution of the spinor order parameter from Eq. (2.10) during vortex pumping in a setup where the harmonic trap is combined with a strong plug potential of the form of Eq. (3.11). The plug is chosen to have the amplitude $A = 100\hbar\omega_r$ and width $d = 3a_r$, and thus it is considerably stronger than that used in Ref. [73] ($A = 10\hbar\omega_r$ and $d = 2a_r$), where unsplit vortices up to $\kappa = 8$ were reached. Otherwise, the systems considered in Publication III and Ref. [73] are identical; in particular, the control cycle is the one presented in Fig. 3.1.

Figure 3.5 shows the time dependence of the orbital angular momentum $\langle \hat{L}_z \rangle = i\hbar \int d^3r \Psi_j^* \left(\mathbf{r}\right) \left(y\partial_x - x\partial_y\right) \Psi_j \left(\mathbf{r}\right)$ of the BEC during the pumping simulation. A symmetric 20-quantum vortex is obtained in the middle of the ninth cycle at $t = 8.5T$. After $t = 9T$, the dissociation of the giant vortex begins in spite of the plug, causing single vortices to move out of the condensate. This is manifested in Fig. 3.5 by the gradual decrease of $\langle \hat{L}_z \rangle$. Nevertheless, the simulation shows that a giant vortex with a very large quantum number κ can be created by pumping if a sufficiently strong optical plug is utilized and the temperature is kept low enough such that dissipation effects due to the thermal gas are negligible.

4. Vortex Clusters

We saw in the previous chapter that multiquantum vortices are prone to divide into several single-quantum vortices. In this chapter, we use states that contain more than one vortex as a starting point for the study. In Sec. 4.1, we discuss vortex dipoles, pairs of vortices and antivortices, focusing on the results of Publication IV and their relation to recent experiments. In Sec 4.2, we describe how a system of two attractively interacting BECs can produce unconventional vortex lattices as a response to external rotation.

4.1 Quantized vortex dipoles

A vortex dipole in a classical or quantum fluid consists of a pair of vortices of opposite circulation, i.e., a vortex and an antivortex, with the dynamics of each vortex line influenced by the fluid flow pattern of the other vortex. Whereas single vortices carry angular momentum, vortex dipoles can be viewed as basic topological entities that are able to carry linear momentum. Although vortex dipoles are widespread in classical fluid flows [147], their role in superfluids seems less well established. Given the appearance of vortices and antivortices in the Berezinskii–Kosterlitz–Thouless transition of two-dimensional superfluids [29, 148–153] and superfluid turbulence [154–156], a detailed study of vortex dipoles will contribute to a broader understanding of superfluid phenomena.

The realization of vortex dipoles in atomic BECs is particularly important as the condensates provide a clean testing ground for vortex physics. In this context, simulations based on the GP equation have shown that vortex dipoles are nucleated when the BEC moves past an impurity faster than a critical velocity, above which the emergence of vortices induces a drag force [157, 158]. Vortex dipoles are hence believed to provide a mech-

anism for the breakdown of superfluidity [159–161].

Quantized vortex dipoles were recently observed for the first time in a BEC experiment by Neely *et al.* [146]. The dipoles were nucleated by forcing superfluid flow around a repulsive Gaussian plug potential within the BEC. The observations were accompanied by a numerical integration of the GP equation, which achieved good agreement with the experimental vortex trajectories.

The presence of the trapping potential in the atomic BECs allows for the existence of peculiar vortex-cluster states that are stationary in the laboratory frame of reference without any external rotation. Let us consider the vortex dipole, and denote the separation distance between the vortex and the antivortex by $d_{\rm sep}$, and let $E_{\rm vd}\,(d_{\rm sep})$ be the minimum energy of the trapped condensate with the restriction that the distance of the phase singularities is $d_{\rm sep}$. The ground state of the system is obtained in the limit $d_{\rm sep} \to 0$, and thus, $E_{\rm vd}$ is an increasing function of $d_{\rm sep}$ for sufficiently small $d_{\rm sep}$. On the other hand, the ground state also corresponds to the limit $d_{\rm sep} \to \infty$. Consequently, there must exist at least one point $d_{\rm sep}^{\rm c}$ which is a local maximum of $E_{\rm vd}\,(d_{\rm sep})$. This maximum indicates the existence of a stationary, energetically unstable vortex-dipole state at the separation $d_{\rm sep}$. Based on similar reasoning, other vortex cluster configurations that are stationary in nonrotated BECs and consist of a greater number of phase singularities, such as vortex tripoles and vortex quadrupoles, have also been predicted and analyzed [162–165]. Furthermore, vortex tripoles have been observed in a recent experiment where vortices were generated using oscillating magnetic quadrupole fields [166].

The stationary vortex dipole was realized experimentally by Freilich *et al.* [82]. In the experiment, vortices were spontaneously created during evaporative cooling due to the Kibble–Zurek mechanism [167, 168], in which the rapid quench of a cold thermal gas through the BEC phase transition results in the appearance of topological defects [169–171], and the orbital dynamics of single vortices and vortex dipoles were measured with high precision. The observations were done with a novel method of vortex probing that allows vortex dynamics to be observed in real time during a single experimental run rather than by reconstruction of images from several runs.[1] The method is based on repeated extraction, expansion, and

[1]Typically, vortices have been imaged by removing the trapping potential and expanding the condensate in order to make the vortex cores optically resolvable,

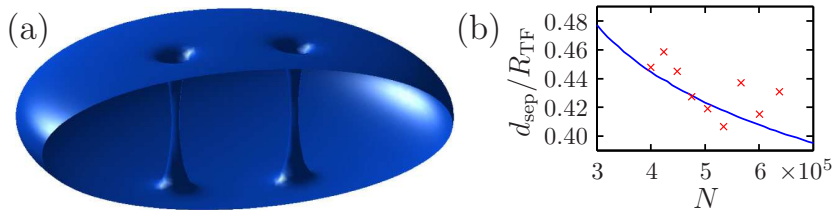

Figure 4.1. Stationary vortex dipole in three dimensions. (a) The isosurface of the particle density $|\Psi(\mathbf{r})|^2$ for the stationary vortex dipole corresponding to the particle number $N = 5 \times 10^5$. Here, d_{sep} is the separation distance between the vortex cores and R_{TF} is the Thomas–Fermi radius of the condensate. (b) The ratio $d_{\mathrm{sep}}/R_{\mathrm{TF}}$ as a function of N. The red crosses represent the experimental data of Ref. [82].

imaging of small fractions (1 to 10%) of the BEC. In the experiment, up to nine images of a single BEC were taken. This enabled Freilich *et al.* to obtain compelling experimental evidence for stationary vortex dipoles. In addition, they were able to accurately measure the separation distance d_{sep} of the dipole in the stationary state.

Previously published predictions [164, 165, 172–174] for the sizes of stationary vortex dipoles concern only very weakly interacting or pancake-shaped condensates and hence cannot be directly compared with the data of Ref. [82]. In Publication IV, we present stationary vortex-dipole states for a BEC identical to the one used by Freilich *et al.* and find excellent quantitative agreement with the experiment. The stationary vortex dipoles are solved from the three-dimensional time-independent GP equation for a range of particle numbers N corresponding to the experiment. The results are summarized in Fig. 4.1. As can be observed from Fig. 4.1(b), the experimental values of Freilich *et al.* are within a few percent of the numerically obtained separation distance. We stress that the numerical curve in Fig. 4.1(b) is drawn without any fitting parameters, and that there is actually an estimated 10% uncertainty in the measurement of the particle number N.

In addition to stationary vortex dipoles, Freilich *et al.* also investigated the orbital motion of nonstationary asymmetric vortex dipoles, with one vortex near the center of the BEC and the other close to the surface [82]. In Publication IV, we perform a related simulation by first placing the vortex cores at the experimentally measured initial positions and then letting the state evolve according to the GP equation. We also study the effect of the multishot imaging method on the dynamics by reducing the

which prevents taking multiple images from a single BEC.

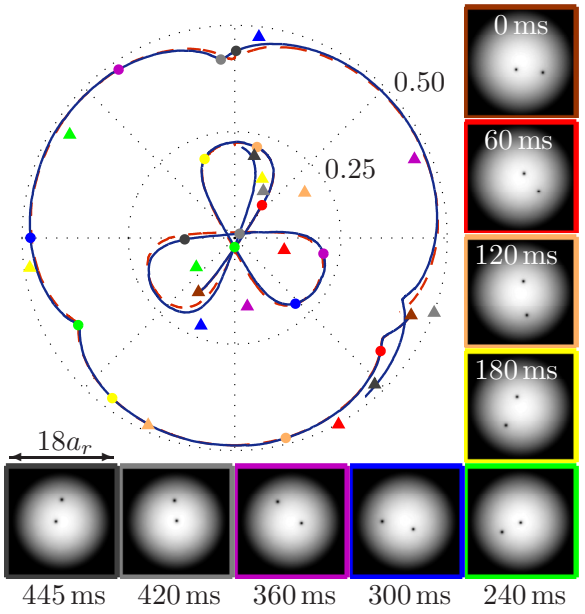

Figure 4.2. Trajectories $(x_\mathrm{v}/R_\mathrm{TF}, y_\mathrm{v}/R_\mathrm{TF})$ of vortices for an asymmetric vortex dipole when $5\,\%$ of the atoms are removed every 60 ms from the state (blue curves). The red curve shows the trajectories when no particles are removed. The insets depict the density $|\Psi(x,y)|^2$ at each moment of particle extraction; these time instants are indicated by solid circles. The triangles designate the experimental measurements of Ref. [82] for the same time instants and initial configurations. The marker colors correspond to the image frames.

value of N by 5% every time particles are removed for imaging. An example of the obtained vortex trajectories is presented in Fig. 4.2. We find that the vortices move along approximately periodic trajectories whose exact shapes depend strongly on the initial vortex positions.[2] The atom removal speeds up the vortex motion and excites the breathing mode of the condensate with the characteristic frequency $f_\mathrm{BM} = 2\omega_r/2\pi$ but does not alter the underlying structure of the paths.

Publication IV explains the experimental observations by Freilich *et al.* [82]. In particular, the numerical results for the sizes of the stationary vortex dipoles are in excellent agreement with their data. In light of Fig. 4.2, the real-time imaging method appears to be a promising tool for studying vortex dynamics in trapped BECs: the spatially uniform extraction of particles is found to cause only isotropic size oscillations of the BEC, which can be subtracted from the data at will by a global distance scaling. However, a full exploration of the imaging technique and its effect

[2]Recently, Middelkamp *et al.* have analyzed in detail the motion of nonstationary vortex dipoles both theoretically and experimentally [175].

on vortex dynamics awaits a rigorous description of the particle-extraction process and is beyond the scope of Publication IV.

4.2 Vortex lattices in two-species condensates

An important issue in vortex physics is to elucidate the vortex phases in BECs that consist of more than one component [176]. Multicomponent condensates allow the formation of various unconventional topological defects such as those discussed in Sec. 3.1 for the three-component spin-1 condensates. Even for the simpler two-component BEC, a rich variety of ground-state vortex phases have been found in theoretical studies. These include coreless vortices [177, 178], serpentine vortex sheets [179], giant skyrmions [180, 181], and interlacing square vortex lattices [181–187]. Since it is possible to load and cool two different atomic isotopes in the same trap [188–195], or atoms in two different hyperfine spin states [44, 196–200], two-component BECs can be realized experimentally. To date, the singly quantized coreless vortices [44] and the square lattices [196] have been observed in the laboratory.

In Publication V, we study vortex lattices in rotating two-component BECs in which the two components have unequal atomic masses and interact attractively with each other. The system is modeled with the coupled two-dimensional GP equations [176]

$$\Big[-\frac{\hbar^2\nabla_{\mathrm{2D}}^2}{2m_j} + \frac{1}{2}m_j\omega_j^2 r^2 + g_j n_j + g_{12}n_{3-j} - \Omega\mathcal{L}_z - \mu_j \Big]\Psi_j(r,\phi) = 0, \quad (4.1)$$

where $n_j = |\Psi_j|^2$, $j \in \{1,2\}$, and $g_{12} \leq 0$ is the attractive intercomponent coupling constant. The z component of the orbital angular momentum operator is given by $\mathcal{L}_z = -i\hbar\partial_\phi$, and Ω is the angular frequency at which the trap is rotated about the z axis. Because the atomic masses m_1 and m_2 of the two components are assumed unequal, it follows from the generalized Feynman relation [106, 201, 202],

$$n_{\mathrm{v},j} = \frac{m_j\Omega}{\pi\hbar}, \quad (4.2)$$

that the areal vortex densities $n_{\mathrm{v},1}$ and $n_{\mathrm{v},2}$ are also unequal. On the other hand, the attractive intercomponent interaction favors states in which vortices of different components lie on top of each other, since it acts to maximize the overlap $\int n_1 n_2 \,\mathrm{d}^2 r$. Thus, the two-component BEC may support unconventional vortex lattice geometries when the atomic mass ratio m_1/m_2 is far from unity and the intercomponent attraction is sufficiently

strong. This kind of system was first studied by Barnett *et al.* [201, 202], but they considered only mass ratios $m_1/m_2 \gtrsim 1$ and thus did not detect any nontriangular vortex lattices.

By numerically solving Eqs. (4.1), we demonstrate that the two-component BEC with $m_1 \neq m_2$ and $g_{12} < 0$ exhibits exotic ground-state vortex configurations in a rotating harmonic trap. The main results are illustrated in Fig. 4.3. For simplicity, we consider here only the mass ratio $m_1/m_2 = 2$ due to its rich variety of lattice structures as well as its experimental relevance—for the already realized mixtures of ^{41}K and ^{87}Rb [188–192], the mass ratio is 2.1, and we have verified numerically that such a system hosts ground-state vortex lattices similar to those found for $\rho = 2$. To emphasize the role of the intercomponent attraction, we consider a range of values for its relative strength $\sigma := -g_{12}/g_1 \in [0, 1)$. In experiments, g_{12} may be controlled with interspecies Feshbach resonances [203], which have been demonstrated for various alkali-metal mixtures [191, 204–206].

At $\sigma = 0$, the components are noninteracting, and the ground state contains triangular lattices in both components. As the intercomponent attraction increases, the ground-state profiles change gradually into square lattices as shown for $\sigma = 0.60$. A further increase in σ eventually recovers the triangular geometry, but with vortex pairs occupying the lattice points in component 1 instead of solitary vortices. Finally, as $\sigma \to 1$, the vortex pairs merge into two-quantum vortices.

The results of Publication V shed light on the hydrodynamics of interacting superfluid mixtures and provide a novel example of a ground-state multiquantum vortex, a structure that rarely exists in nature.[3] Importantly, the square geometry or the double-quantum nature of the lattices is not induced here by external fields [207] but is an inherent property of the system. The exotic lattices can be realized with current experimental techniques [191].

[3] Since the energy of a vortex increases quadratically with its quantum number, multiply quantized vortices do not usually appear in the ground state.

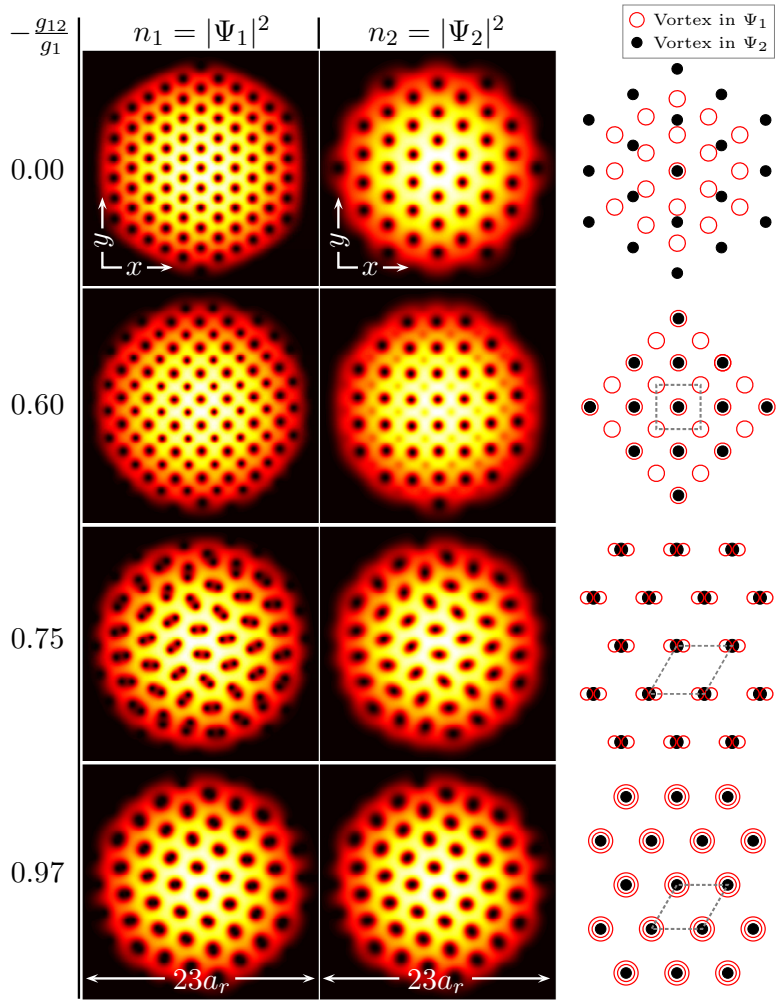

Figure 4.3. Ground-state particle densities n_1 (left column) and n_2 (center column) of a two-component BEC with the mass ratio $m_1/m_2 = 2$ for different values of the intercomponent attraction strength $\sigma := -g_{12}/g_1$. The right column illustrates each lattice geometry, and the unit cell of the combined lattice is shown with dashed grey lines. The rotation frequency is set to $\Omega = 0.97\,\omega_1$ and the total interaction strength is $(g_1 + g_{12})\, N_1/\hbar\omega_1 a_{r,1}^2 = 705$, where $a_{r,1} = \sqrt{\hbar/m_1\omega_1}$.

5. Spin Vortices and Elementary Excitations in Dipolar Bose–Einstein Condensates

During the recent years, long-range dipole–dipole interactions have attracted considerable interest in the study of gaseous BECs [74]. Condensates subject to these anisotropic forces form the subject of this chapter. Section 5.1 generalizes the mean-field theory of Chapter 2 to include the dipolar interactions alongside with the ordinary contact interactions. In Secs. 5.2 and 5.3, we investigate helical spin textures and elementary excitations in dipolar spin-1 BECs. We also summarize and discuss the main results of Publications VI and VII.

5.1 Dipole–dipole interactions in Bose–Einstein condensates

At least three motives for investigating dipolar BECs can be identified:

1. Significant experimental progress has been made in recent years in cooling and trapping of electrically polar molecules [208] and atomic species having large magnetic moments. In the case of polar molecules, several experimental groups utilizing Feshbach-resonance and photoassociation techniques [209–211] have been making significant progress in realizing degenerate gases of polar molecules, which interact dominantly by the electric dipole–dipole forces. In the case of magnetic dipoles, Bose–Einstein condensation of ^{52}Cr, a species with a large atomic magnetic moment of $6\mu_{\mathrm{B}}$, was achieved in 2004 [212] and has since then enabled the first experimental investigations of dipolar quantum gases.

2. The properties of the dipole–dipole interaction are fundamentally different from those of the local density–density and spin–spin interactions considered in previous chapters. Namely, the dipolar interaction is *long-range* (decaying as d^{-3}, where d is the interparticle distance) and

anisotropic. Thus, the dipole–dipole interaction gives rise to a wealth of novel and unexpected effects in BECs.

3. Recent experiments have indicated that dipole–dipole interactions may be important for ferromagnetic spin-1 condensates of ^{87}Rb in the absence of external magnetic fields [75, 76]. In particular, Vengalattore *et al.* [75] demonstrated the spontaneous decay of helical spin textures into spatially modulated structures of spin domains. When the dipolar interactions were reduced by means of radio-frequency pulses, the modulation was suppressed, and thus the effect was ascribed to the dipolar forces. In addition, although the dipole–dipole interactions in alkali-metal condensates are typically weak, it may be feasible to tune their relative strength by utilizing optical Feshbach resonances [213], which have been demonstrated for ^{87}Rb [214].

Let us begin by generalizing the equations of Chapter 2 to include the anisotropic and nonlocal dipole–dipole forces. If such interactions are present in a dilute gas of spin-1 particles and the gas is confined in a purely optical trap, the spin degrees of freedom are coupled to the orbital degrees of freedom. The full grand-canonical Hamiltonian of the system becomes $\hat{K} + \hat{H}_{\mathrm{d}}$, where $\hat{K}$ is defined in Eq. (2.1) and the dipolar term is

$$\hat{H}_{\mathrm{d}} = \frac{g_{\mathrm{d}}}{2} \iint \mathrm{d}^3 r \, \mathrm{d}^3 r' D_{\alpha\beta}(\mathbf{r}-\mathbf{r}') \hat{\psi}_j^\dagger(\mathbf{r}) \hat{\psi}_{j'}^\dagger(\mathbf{r}') F_{jk}^\alpha F_{j'k'}^\beta \hat{\psi}_{k'}(\mathbf{r}') \hat{\psi}_k(\mathbf{r}). \qquad (5.1)$$

The dipolar coupling constant is given by $g_{\mathrm{d}} = \mu_0 \mu_{\mathrm{B}}^2 g_F^2 / 4\pi$, where μ_0 denotes the permeability of vacuum, and the kernel functions are defined as $D_{\alpha\beta}(\mathbf{R}) = \left(\delta_{\alpha\beta} R^2 - 3R_\alpha R_\beta\right)/R^5$ with $\alpha, \beta \in \{x, y, z\}$. Correspondingly, the mean-field GP equation of the dipolar spin-1 BEC becomes a nonlinear integro-differential equation

$$\begin{aligned} i\hbar\partial_t \Psi_j(\mathbf{r},t) \;=\; & \Big[\mathcal{H}_{jk} - \mu\delta_{jk} + g_{\mathrm{n}} \Psi_{j'}^* \Psi_{j'} \delta_{jk} + g_{\mathrm{s}} \Psi_{j'}^* \mathbf{F}_{j'k'} \Psi_{k'} \cdot \mathbf{F}_{jk} \\ & + g_{\mathrm{d}} \int \mathrm{d}^3 r' D_{\alpha\beta}(\mathbf{r}-\mathbf{r}') M^\beta(\mathbf{r}',t) F_{jk}^\alpha \Big] \Psi_k(\mathbf{r},t), \end{aligned} \qquad (5.2)$$

where $M^\beta(\mathbf{r}',t) = \Psi_{j'}^*(\mathbf{r}',t) F_{j'k'}^\beta \Psi_{k'}(\mathbf{r}',t)$ is the β component of the local magnetization. We point out that in general, the dipole–dipole interaction breaks the rotational symmetry of the system in the spin space. Consequently, the dipolar interaction does not necessarily conserve the total magnetization of the BEC.

The Bogoliubov equation also becomes nonlocal in the presence of dipolar forces. Let us define a linear functional $\mathcal{L}_{\alpha\beta}[f](\mathbf{r}) := \int \mathrm{d}^3 r' D_{\alpha\beta}(\mathbf{r} -$

$\mathbf{r}')f(\mathbf{r}')$ and denote $(\mathcal{L}_{\alpha\beta}\circ g)\,f \equiv \mathcal{L}_{\alpha\beta}[gf](\mathbf{r})$, where $f(\mathbf{r})$ and $g(\mathbf{r})$ are arbitrary functions. With this notation, the dipolar Bogoliubov equation is written as

$$\begin{pmatrix} \mathcal{A}_{jk}+\mathcal{A}^{\mathrm{d}}_{jk} & \mathcal{B}_{jk}+\mathcal{B}^{\mathrm{d}}_{jk} \\ -\mathcal{B}^{*}_{jk}-\mathcal{B}^{\mathrm{d}*}_{jk} & -\mathcal{A}^{*}_{jk}-\mathcal{A}^{\mathrm{d}*}_{jk} \end{pmatrix} \begin{pmatrix} u_{q,k}(\mathbf{r}) \\ v_{q,k}(\mathbf{r}) \end{pmatrix} = \hbar\omega_q \begin{pmatrix} u_{q,j}(\mathbf{r}) \\ v_{q,j}(\mathbf{r}) \end{pmatrix}, \tag{5.3}$$

where the nonlocal dipolar terms are given by

$$\mathcal{A}^{\mathrm{d}}_{jk} = g_{\mathrm{d}}\left(\mathcal{L}_{\alpha\beta}\left[\Psi^{*}_{j'}F^{\beta}_{j'k'}\Psi_{k'}\right]F^{\alpha}_{jk} + F^{\alpha}_{jk'}\Psi_{k'}\mathcal{L}_{\alpha\beta}\circ\Psi^{*}_{j'}F^{\beta}_{j'k}\right), \tag{5.4}$$

$$\mathcal{B}^{\mathrm{d}}_{jk} = g_{\mathrm{d}}F^{\alpha}_{jk'}\Psi_{k'}\mathcal{L}_{\alpha\beta}\circ\Psi_{j'}\left(F^{\beta}_{j'k}\right)^{*}. \tag{5.5}$$

In Publication VII, Eq. (5.3) is solved in the quasi-two-dimensional pancake geometry.

5.2 Helical spin textures in dipolar condensates

Spin textures with helical geometries, and their relation to dipolar interactions, have recently drawn attention in the study of spinor BECs. In a recent experiment by Vengalattore *et al.* [75], a helical magnetization texture in a quantum degenerate gas of ferromagnetic spin-1 $^{87}\mathrm{Rb}$ was observed to decay spontaneously into small spin domains, and the effect was argued to result from the weak dipolar forces between the atoms. Earlier theoretical studies have shown that the long-range dipolar interactions can stabilize spin-vortex states in various geometries [77–79] and that even weak dipolar interactions can lead to dynamic formation of a helical spin texture in a ferromagnetic spin-1 BEC [81]. Moreover, in a classical spin approximation corresponding to ferromagnetic systems with large magnetic moments, the spin helix has been found to be the ground-state texture in a suitable geometry and with strong enough dipolar interactions [80].

In Publication VI, we investigate elongated helical spin textures in ferromagnetic spin-1 BECs with dipolar interparticle forces. Using Eq. (5.2) to model the condensate, we seek stationary helical states under the assumption that the system is infinitely long in the direction of the helix axis and find solutions hosting different types of topological line defects, i.e., quantized vortices. Due to the symmetry of the order-parameter field, these line defects encircle the condensate in a helical pattern. Rather than fixing the dipolar coupling constant g_{d} to some predetermined value, we present results for various interaction strengths in order to emphasize the role of the dipolar interactions.

The assumption that the system is infinitely long in the axial direction allows a well-defined wave vector κ_{h} for the helical texture. In order to analyze the helices numerically, we fix κ_{h} and calculate the energy-minimizing texture in a plane subject to the condition that the planar texture is mapped along the axial z direction according to the helical structure. Thus, we search for stationary solutions to Eq. (5.2) of the form

$$\Psi(r,\phi,z) = e^{iq_z z} e^{i\kappa_{\mathrm{h}} z F_z} \Psi\left(r, \phi + \kappa_{\mathrm{h}} z, 0\right) \tag{5.6}$$

where (r,ϕ,z) are the cylindrical coordinates and q_z is a Bloch wave vector that accounts for the effective periodic potential in the z direction. With this ansatz, Eq. (5.2) is reduced to a two-dimensional equation in which the dipolar potential can be efficiently evaluated by carrying out a series of one-dimensional Hankel transforms.

By numerically solving the resulting GP equation for different values of κ_{h}, we find two classes of helical solutions referred to as the *Mermin–Ho vortex helix* and the *polar-core vortex helix*. Examples of these states are presented in Figs. 5.1(a)–(f). Figure 5.1(g) illustrates the general structure of the helical solution. The Mermin–Ho vortex helix hosts two Mermin–Ho vortices with phase windings $(0,1,2)$ and $(-2,-1,0)$ in the components $(\Psi_1,\Psi_0,\Psi_{-1})$, respectively (cf. Sec. 3.1). The two vortices carry both spin and mass currents: the spin currents flow in the same direction, whereas the mass currents flow in opposite directions. The polar-core vortex helix contains two spin vortices with the same phase windings $(-1,0,1)$ in the components $(\Psi_1,\Psi_0,\Psi_{-1})$, respectively. The spin vortices have polar core regions, and they carry a spin current but no mass current.

Figure 5.1(h) shows the total energy in these two types of states as a function of the helical wave vector κ_{h}. Whereas the energy of the polar-core vortex is found to be a monotonously increasing function of κ_{h}, the energy of the Mermin–Ho vortex helix is minimized for a finite wave vector κ_{min}. This minimum persists in the total energy for all positive values of g and g_{d} considered in Publication VI and becomes more pronounced with increasing g_{d}.

The helical textures that we find for $F=1$ are in qualitative agreement with those found earlier using the classical spin approach [80], which is supposed to be an accurate model for ferromagnetic systems in the limit of large magnetic moments. Therefore, it is reasonable to expect that similar helical structures exist independent of the value of the atomic spin number F. Publication VI can consequently elucidate phenomena in

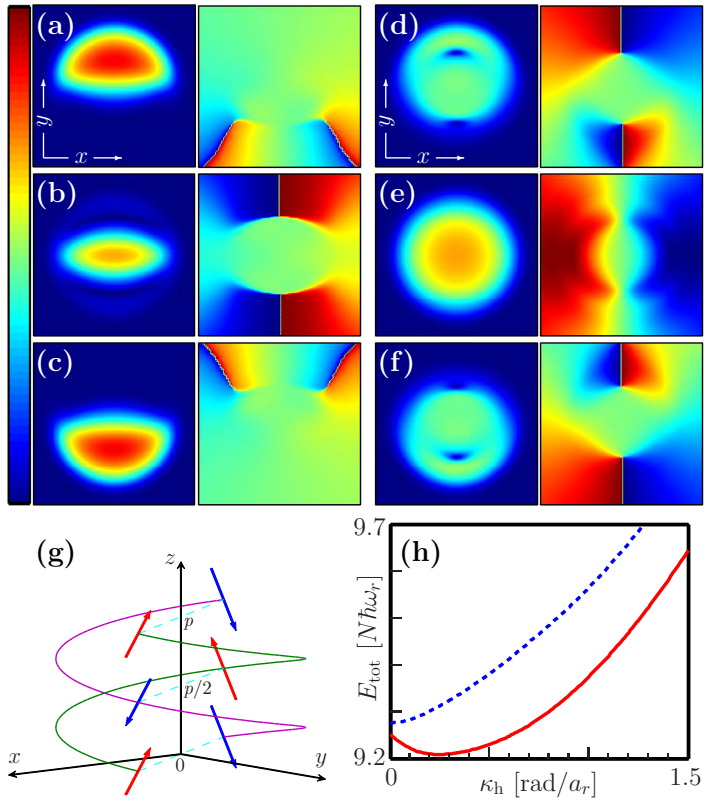

Figure 5.1. Spin helices in dipolar spin-1 condensates. (a)–(c) The amplitudes (left panels) and complex phases (right panels) of the order parameter components Ψ_1, Ψ_0, and Ψ_{-1} for (a)–(c) a Mermin–Ho vortex helix with the helical wave vector $\kappa_{\rm h} = 0.25\,{\rm rad}/a_r$; (d)–(f) a polar-core vortex helix with $\kappa_{\rm h} = 0.25\,{\rm rad}/a_r$. The field of view in each panel is $14a_r \times 14a_r$, and the colormap range is $[0, \max n\,(\mathbf{r})]$ in the left panels and $[0, 2\pi]$ in the right panels. (g) A schematic illustration of the spin-helix state [Eq. (5.6)]. Here, $p = 2\pi/\kappa_{\rm h}$ denotes the pitch of the helix. The arrows point in the direction of the local spin. Single points in the plane $z = 0$ are mapped to helical trajectories depicted by the solid curves. (h) The total energy as a function of $\kappa_{\rm h}$ for the Mermin–Ho vortex (solid) and the polar-core vortex (dashed) helices.

strongly dipolar systems with more complex order parameters, such as in the spin-3 gas of ^{52}Cr [215].

The helical spin textures discovered in Publication VI are most transparent in elongated, cigar-shaped BECs. One difficulty in observing them as stable configurations in a condensate with weak dipolar interactions, such as ^{87}Rb, is that the spins tend to align predominantly parallel to the weak axis of the trap due to the head-to-tail attraction of the dipoles [77, 79, 80]. However, by performing additional three-dimensional simulations, we show that this problem can be overcome by placing the cigar-shaped system in a one-dimensional optical lattice potential along the weak axis of the trap, say, the z axis. In the simulations, we calculate the energies of an axially spin-polarized state and a helical spin texture as functions of the strength of the optical lattice potential, observing that the helical texture becomes the lower-energy state as the lattice strength is increased. This behavior is understood as follows: A strong enough lattice deforms the elongated condensate into a series of pancake-shaped clouds. Within each cloud, the preferred direction of magnetization lies in the xy plane, and the relative orientation of magnetization between neighboring clouds is determined by the long-range dipolar forces, which favor the helical ordering.

5.3 Elementary excitations in dipolar condensates

The study of collective excitations (Sec. 2.4) has played an important role in probing the physics of atomic BECs. Recently, various studies have addressed the question of how dipolar interactions affect the elementary excitation spectra of dilute BECs. Theoretically, the dipolar interactions have been shown to give rise to novel collapse dynamics [216] and the roton–maxon instability [217], and a dipolar shift in the frequency of a collective density oscillation has been observed experimentally [218]. These studies concern spin-polarized dipolar condensates, which are described by a scalar order-parameter field. In Publication VII, we present the first investigation of elementary excitations in dipolar BECs that fully incorporates the spin degree of freedom into the model.

We use the spin-1 mean-field model, Eq. (5.2), to numerically study the low-energy excitation spectra of ferromagnetic dipolar condensates. In order to make the numerical solution of Eq. (5.3) feasible, we assume that the BEC is tightly confined in the z direction such that the order param-

eter can be factorized as $\Psi(\mathbf{r},t) = \Psi(x,y,t)\zeta_0(z)$. This approximation implies that the magnetization does not depend on z, and it should be accurate in the limit $\omega_z \gg \omega_r$. Due to the nonlocality of the dipolar interaction potentials, the resulting Bogoliubov matrix is not generally a sparse matrix, and its explicit diagonalization becomes cumbersome. To avoid this problem, we use the Arnoldi iteration that relies on repetitive operation by the system matrix without the need to store it in memory. Each operation by the matrix requires the evaluation of two-dimensional dipolar integrals, which we implement efficiently with a fast Fourier transform.

The elementary excitations are solved for three types of stationary states [Figs. 5.2(a)–(c)]. We consider a spin-vortex state and an almost spin-polarized, so-called flare state in the absence of external magnetic fields. In addition, we calculate the excitations for a state in which the atomic spins are polarized perpendicular to an external field and are precessing rapidly about it with the Larmor frequency ω_{L}.

The elementary excitations can be assigned a quantum number $l \in \mathbb{Z}$ that determines the phase winding of the quasiparticle amplitude with respect to the stationary state.[1] Typically, the lowest-energy excitations are those with small values of l, such as $l = 0$ (the breathing mode), $l = \pm 1$ (dipole modes), or $l = \pm 2$ (quadrupole modes). Moreover, in the absence of dipolar interactions, the excitations can be classified into density waves, spin waves and magnetic quadrupole waves, depending on whether they induce oscillations mainly in the density n, the magnetization $\mathbf{M}$, or the magnetic quadrupole tensor $Q_{\alpha\beta} = 2\delta_{\alpha\beta}/3 - \langle F^\alpha F^\beta + F^\beta F^\alpha \rangle / 2n$, respectively.

The main results of Publication VII are presented in Fig. 5.2, which illustrates the three types of stationary states considered and shows their excitation energies as functions of the dipolar coupling strength g_{d}. For clarity, we have presented the energies only for selected lowest-energy excitation modes. In the limit $g_{\mathrm{d}}/g_{\mathrm{n}} \to 0$, the three highest-energy modes in Figs. 5.2(d)–(f) are the density breathing ($l = 0$), density quadrupole ($l = \pm 2$), and density dipole ($l = \pm 1$) modes, in order of descending energy. The three lower-lying modes consist of the lowest magnetic quadrupole oscillation ($l = 0$) and spin waves ($l = \pm 2$ and $l = \pm 1$).

Figure 5.2 reveals that in general, excitations that induce mainly density fluctuations are relatively robust against changes in the dipolar coupling strength. In particular, the excitation energy of the density dipole

[1] In Publication VII, this quantum number is denoted by κ.

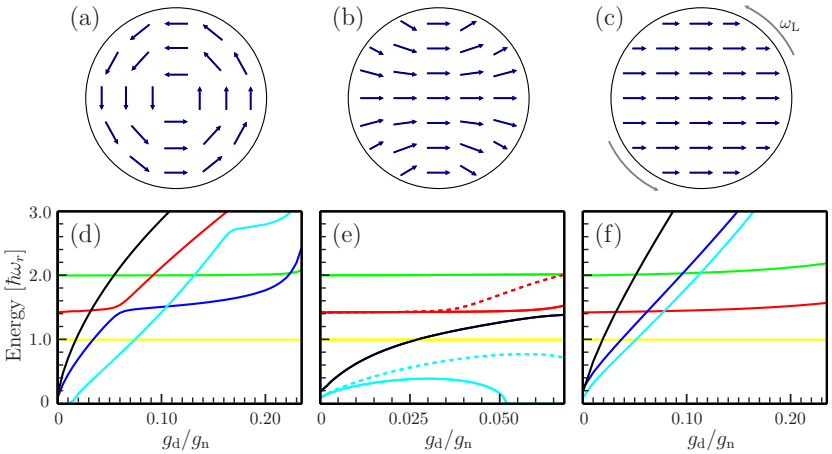

Figure 5.2. Stationary states studied in Publication VII and their excitation spectra. The top row illustrates the three spin textures under consideration: (a) *spin vortex*, (b) *flare*, and (c) *spin-polarized state*. The spin vortex and flare are studied in the absence of magnetic fields, whereas the spins in the polarized state are precessing rapidly with the Larmor frequency ω_L about a homogeneous field perpendicular to the plane of the figure. The bottom row shows the excitation energies of selected Bogoliubov modes as functions of the dipolar coupling strength g_d for (d) the spin vortex, (e) the flare, and (f) the spin-polarized state.

mode is determined solely by the external trapping potential, and hence it is independent of g_d. The energy of the density breathing mode similarly shows only weak dependence on g_d. On the other hand, the excitation energies of the magnetic quadrupole mode and the spin waves are observed to increase rapidly with g_d.

We also find that the density and spin oscillations become mixed due to the long-range anisotropic dipolar forces. In the limit $g_d/g_n \to 0$, only the density oscillations impart significant density modulations. However, as the dipolar coupling strength increases, even the spin waves start producing density modulations. In fact, when an avoided crossing occurs at $g_d/g_n \approx 0.06$ in Fig. 5.2(d) for the density and spin waves of the same quantum number $l = \pm 2$, the density waves transform into spin waves and vice versa.

Publication VII provides the first study of elementary excitations in a harmonically trapped, pancake-shaped BEC with dipolar interactions and full spin dynamics included in the model. Since the stationary states studied in Publication VII have analogous counterparts in the classical spin approach that describes condensates of particles with large dipole moments, our results may also be applicable to strongly dipolar systems.

6. Summary and Conclusions

Ever since the realization of the first dilute atomic Bose–Einstein condensates in 1995, there has been a surge in the research activity in atomic physics, due to the numerous prospects and challenges provided by these coherent quantum systems. The atomic BECs have opened up the possibility to model an interacting many-particle system from first-principles quantum theories and have enabled experimentalists to realize a number of exotic phenomena that have proven elusive in their original context—a prominent example is the quantized vortex, which was first proposed to exist in superfluid helium.

In the research presented in this dissertation, the main objective was to study exotic, yet experimentally relevant, vortex structures in dilute Bose–Einstein condensates. The specific topics tackled during the research consisted of multiquantum vortices and vortex dipoles in spin-polarized condensates, vortex lattices in a system of two attractively interacting condensates, and spin textures in condensates with dipolar interactions. Theoretical and computational methods were used to analyze the energetics, stability, and dynamics of these structures in a harmonic trap in the zero-temperature limit.

A central research question, motivated by the recently proposed vortex pump [73], concerned the creation and properties of giant vortices with large quantum numbers. In Publications I–III, the size, dynamical stability, and splitting of such vortices were studied using the zero-temperature mean-field theory. It was found that although giant vortices are dynamically unstable against splitting into singly quantized vortices at nearly all values of the atom–atom interaction strength, the strength of this instability saturates to a fairly low value and can be reduced to zero by employing an experimentally realizable optical potential. On the other hand, the observed increase of the vortex core radius r_{c} with the vortex

quantum number κ as $r_c \propto \sqrt{\kappa}$ makes it possible to gradually increase the pumping speed without compromising the adiabaticity of the process. Together these findings suggest that multiquantum vortices of very high angular momenta may be achieved with the pump. Since such vortices would provide access to the novel splitting patterns discovered in Publication II and open up the possibility to study the proposed connection between giant-vortex splitting and superfluid turbulence [219, 220], the experimental realization of the vortex pump would be an important milestone in vortex physics.

In a recent pioneering experiment, Freilich *et al.* measured vortex dynamics in real time and were able to obtain convincing evidence for a stationary vortex dipole [82]. Publication IV presented numerical calculations that explained the experimental observations of Freilich *et al.* In particular, the numerically obtained size of the stationary vortex dipole was within a few percent of the experimental value, which confirms that the state observed by Freilich *et al.* really was a genuinely stationary vortex dipole. Previous literature on stationary vortex dipoles considered only weakly interacting or effectively two-dimensional systems, and predictions that could be compared with the experiment did not exist until Publication IV.

Publication V was devoted to studying vortex lattices in harmonically trapped, rotating two-component BECs in which the components have unequal atomic masses and interact attractively with each other. Such systems were found to exhibit unconventional ground-state vortex configurations, such as vortex lattices with square geometry or lattices consisting of vortex pairs or two-quantum vortices, if the ratio of the atomic masses was suitable. The vortex-pair lattice and the two-quantum-vortex lattice are novel ground-state structures of Bose–Einstein-condensed systems and contribute to our understanding of how interacting superfluid mixtures respond to rotation. The lattices should be realizable in the two-species BEC of ^{41}K and ^{87}Rb with current experimental techniques [191].

In Publications VI and VII, elonganted spin helices and elementary excitations were investigated in spin-1 BECs with dipole–dipole interactions. Two classes of helical spin textures were discovered, the Mermin–Ho and the polar-core vortex helix, each texture containing two spin vortices of the type suggested by the name. The dipolar interactions were found to stabilize the Mermin–Ho vortex helix for a finite helical pitch. In Publication VII, the energies of spin-wave excitations were found to increase

rapidly with the dipolar coupling strength, whereas the energies of density oscillations changed only slightly.

The results of Publications VI and VII are in line with earlier studies that have reported a stabilizing effect of the dipolar interactions on various spin textures [77,221–223]. Furthermore, because the states analyzed here for the hyperfine spin $F = 1$ have counterparts in the classical spin approach that describes condensates of particles with very large values of F [80, 224], the results of Publications VI and VII are expected to shed light on the behavior of strongly dipolar systems with more complex order parameters, such as the $F = 3$ condensate of ^{52}Cr or the recently realized $F = 8$ condensate of the most magnetic element, ^{164}Dy [225].

This dissertation includes original, experimentally realizable results on unconventional vortex configurations in dilute Bose–Einstein condensates. These results cover, e.g., novel splitting patterns of giant vortices, exotic ground-state vortex lattices in rotating condensate mixtures, and helical spin-vortex states in dipolar condensates. Taken together, these findings deepen our understanding of superfluid and vortex phenomena in the dilute condensates. The results also contribute to the search for novel vortex structures in present-day experiments.

In future research, it would be interesting to extend the stability analysis of the giant vortices and the study of their splitting to three-dimensional or anharmonic trap configurations, to investigate the exotic lattices analytically in the limit of very fast rotation, and to probe the effect of trapping on the roton-maxon spectrum in the dipolar condensates. Moreover, the research presented in this dissertation has been performed exclusively using the zero-temperature formalism. In order to study the possible finite-temperature effects, one could utilize, e.g, the Hartree–Fock–Bogoliubov–Popov approximation [226, 227], classical field methods [228], or the Zaremba–Nikuni–Griffin formalism [229].

At the present time, we can only speculate as to what the gaseous BECs will be used for in the future. Come what may, these ideal quantum laboratories will continue to fascinate the minds of physicists for years to come.

Bibliography

[1] S. N. Bose, Z. Phys. **26**, 178 (1924).

[2] A. Einstein, Sitzungber. Kgl. Preuss. Akad. Wiss. **1924**, 261 (1924).

[3] A. Einstein, Sitzungber. Kgl. Preuss. Akad. Wiss. **1925**, 3 (1925).

[4] P. Kapitza, Nature **141**, 74 (1938).

[5] J. F. Allen and A. D. Misener, Nature **141**, 75 (1938).

[6] F. London, Phys. Rev. **54**, 947 (1938).

[7] F. London, Nature **141**, 643 (1938).

[8] P. Sokol, in *Bose–Einstein Condensation*, edited by A. Griffin, D. W. Snoke, and S. Stringari (Cambridge University Press, Cambridge, 1995).

[9] D. M. Ceperley, Rev. Mod. Phys. **67**, 279 (1995).

[10] J. Bardeen, L. N. Cooper, and J. R. Schrieffer, Phys. Rev. **108**, 1175 (1957).

[11] J. R. Schrieffer, *Theory of Superconductivity* (Perseus Books, Reading, 1999).

[12] S. Stenholm, Rev. Mod. Phys. **58**, 699 (1986).

[13] S. Chu, Rev. Mod. Phys. **70**, 685 (1998).

[14] C. N. Cohen-Tannoudji, Rev. Mod. Phys. **70**, 707 (1998).

[15] W. D. Phillips, Rev. Mod. Phys. **70**, 721 (1998).

[16] M. H. Anderson, J. R. Ensher, M. R. Matthews, C. E. Wieman, and E. A. Cornell, Science **269**, 198 (1995).

[17] K. B. Davis, M. O. Mewes, M. R. Andrews, N. J. van Druten, D. S. Durfee, D. M. Kurn, and W. Ketterle, Phys. Rev. Lett. **75**, 3969 (1995).

[18] C. C. Bradley, C. A. Sackett, J. J. Tollett, and R. G. Hulet, Phys. Rev. Lett. **75**, 1687 (1995).

[19] *Press Release: The 2001 Nobel Prize in Physics*, Nobelprize.org, 9 October 2001, available online at `http://www.nobelprize.org/nobel_prizes/physics/laureates/2001/press.html` (viewed 3 September 2012).

[20] Y. Castin, J. Dalibard, and C. Cohen-Tannoudji, in *Bose–Einstein Condensation*, edited by A. Griffin, D. W. Snoke, and S. Stringari (Cambridge University Press, Cambridge, 1995).

[21] C. E. Wieman, D. E. Pritchard, and D. J. Wineland, Rev. Mod. Phys. **71**, S253 (1999).

[22] H. J. Metcalf and P. van der Straten, *Laser Cooling and Trapping* (Springer-Verlag, New York, 1999).

[23] C. J. Pethick and H. Smith, *Bose-Einstein Condensation in Dilute Gases* (Cambridge University Press, Cambridge, 2008).

[24] S. Inouye, M. R. Andrews, J. Stenger, H.-J. Miesner, D. M. Stamper-Kurn, and W. Ketterle, Nature **392**, 151 (1998).

[25] M.-O. Mewes, M. R. Andrews, D. M. Kurn, D. S. Durfee, C. G. Townsend, and W. Ketterle, Phys. Rev. Lett. **78**, 582 (1997).

[26] B. P. Anderson and M. A. Kasevich, Science **282**, 1686 (1998).

[27] I. Bloch, T. W. Hänsch, and T. Esslinger, Phys. Rev. Lett. **82**, 3008 (1999).

[28] M. Greiner, O. Mandel, T. Esslinger, T. W. Hänsch, and I. Bloch, Nature **415**, 39 (2002).

[29] Z. Hadzibabic, P. Kruger, M. Cheneau, B. Battelier, and J. Dalibard, Nature **441**, 1118 (2006).

[30] U. Leonhardt and P. Piwnicki, Phys. Rev. Lett. **84**, 822 (2000).

[31] L. J. Garay, J. R. Anglin, J. I. Cirac, and P. Zoller, Phys. Rev. Lett. **85**, 4643 (2000).

[32] J. R. Anglin and W. H. Zurek, Phys. Rev. Lett. **83**, 1707 (1999).

[33] D. O'Dell, S. Giovanazzi, G. Kurizki, and V. M. Akulin, Phys. Rev. Lett. **84**, 5687 (2000).

[34] L. D. Landau, J. Phys. USSR **5**, 71 (1941).

[35] L. D. Landau, J. Phys. USSR **11**, 91 (1947).

[36] R. J. Donnelly, *Quantized Vortices in Helium II* (Cambridge University Press, Cambridge, 1991).

[37] D. Vollhardt and P. Wölfle, *The Superfuid Phases of Helium 3* (Taylor and Francis, London, 1990).

[38] *Superconductivity*, edited by R. D. Parks (Marcel Dekker, New York, 1969).

[39] P. W. Anderson and N. Itoh, Nature **256**, 25 (1975).

[40] T. W. B. Kibble, J. Phys. A: Math. Gen. **9**, 1387 (1976).

[41] G. A. Swartzlander and C. T. Law, Phys. Rev. Lett. **69**, 2503 (1992).

[42] G. N. Fowler, S. Raha, and R. M. Weiner, Phys. Rev. C **31**, 1515 (1985).

[43] A. L. Fetter, Rev. Mod. Phys. **81**, 647 (2009).

[44] M. R. Matthews, B. P. Anderson, P. C. Haljan, D. S. Hall, C. E. Wieman, and E. A. Cornell, Phys. Rev. Lett. **83**, 2498 (1999).

[45] B. P. Anderson, J. Low Temp. Phys. **161**, 574 (2010).

[46] R. J. Dodd, K. Burnett, M. Edwards, and C. Clark, Phys. Rev. A **56**, 587 (1997).

[47] D. S. Rokhsar, Phys. Rev. Lett. **79**, 2164 (1997).

[48] H. Pu, C. K. Law, J. H. Eberly, and N. P. Bigelow, Phys. Rev. A **59**, 1533 (1999).

[49] T. Isoshima and K. Machida, Phys. Rev. A **60**, 3313 (1999).

[50] A. A. Svidzinsky and A. L. Fetter, Phys. Rev. Lett. **84**, 5919 (2000).

[51] S. M. M. Virtanen, T. P. Simula, and M. M. Salomaa, Phys. Rev. Lett. **86**, 2704 (2001).

[52] Y. Kawaguchi and T. Ohmi, Phys. Rev. A **70**, 043610 (2004).

[53] A. D. Jackson, G. M. Kavoulakis, and E. Lundh, Phys. Rev. A **72**, 053617 (2005).

[54] J. A. M. Huhtamäki, M. Möttönen, and S. M. M. Virtanen, Phys. Rev. A **74**, 063619 (2006).

[55] E. Lundh and H. M. Nilsen, Phys. Rev. A **74**, 063620 (2006).

[56] P. Capuzzi and D. M. Jezek, J. Phys. B: At. Mol. Opt. Phys. **42**, 145301 (2009).

[57] D. M. Stamper-Kurn, M. R. Andrews, A. P. Chikkatur, S. Inouye, H.-J. Miesner, J. Stenger, and W. Ketterle, Phys. Rev. Lett. **80**, 2027 (1998).

[58] M. D. Barrett, J. A. Sauer, and M. S. Chapman, Phys. Rev. Lett. **87**, 010404 (2001).

[59] J. Stenger, S. Inouye, D. M. Stamper-Kurn, H. J. Miesner, A. P. Chikkatur, and W. Ketterle, Nature **396**, 345 (1998).

[60] M. M. Salomaa and G. E. Volovik, Rev. Mod. Phys. **59**, 533 (1987).

[61] U. Leonhardt and G. E. Volovik, JETP Lett. **72**, 66 (2000).

[62] F. Zhou, Phys. Rev. Lett. **87**, 080401 (2001).

[63] S. Mukerjee, C. Xu, and J. E. Moore, Phys. Rev. Lett. **97**, 120406 (2006).

[64] A.-C. Ji, W. M. Liu, J. L. Song, and F. Zhou, Phys. Rev. Lett. **101**, 010402 (2008).

[65] H. Zhai, W. Q. Chen, Z. Xu, and L. Chang, Phys. Rev. A **68**, 043602 (2003).

[66] H. T. C. Stoof, E. Vliegen, and U. Al Khawaja, Phys. Rev. Lett. **87**, 120407 (2001).

[67] J.-P. Martikainen, A. Collin, and K.-A. Suominen, Phys. Rev. Lett. **88**, 090404 (2002).

[68] C. M. Savage and J. Ruostekoski, Phys. Rev. A **68**, 043604 (2003).

[69] V. Pietilä and M. Möttönen, Phys. Rev. Lett. **103**, 030401 (2009).

[70] E. Ruokokoski, V. Pietilä, and M. Möttönen, Phys. Rev. A **84**, 063627 (2011).

[71] A. E. Leanhardt, A. Görlitz, A. P. Chikkatur, D. Kielpinski, Y. Shin, D. E. Pritchard, and W. Ketterle, Phys. Rev. Lett. **89**, 190403 (2002).

[72] Y.-J. Lin, R. L. Compton, K. Jimenez-Garcia, J. V. Porto, and I. B. Spielman, Nature **462**, 628 (2009).

[73] M. Möttönen, V. Pietilä, and S. M. M. Virtanen, Phys. Rev. Lett. **99**, 250406 (2007).

[74] T. Lahaye, C. Menotti, L. Santos, M. Lewenstein, and T. Pfau, Rep. Prog. Phys. **72**, 126401 (2009).

[75] M. Vengalattore, S. R. Leslie, J. Guzman, and D. M. Stamper-Kurn, Phys. Rev. Lett. **100**, 170403 (2008).

[76] M. Vengalattore, J. Guzman, S. R. Leslie, F. Serwane, and D. M. Stamper-Kurn, Phys. Rev. A **81**, 053612 (2010).

[77] S. Yi and H. Pu, Phys. Rev. Lett. **97**, 020401 (2006).

[78] Y. Kawaguchi, H. Saito, and M. Ueda, Phys. Rev. Lett. **97**, 130404 (2006).

[79] M. Takahashi, S. Ghosh, T. Mizushima, and K. Machida, Phys. Rev. Lett. **98**, 260403 (2007).

[80] J. A. M. Huhtamäki, M. Takahashi, T. P. Simula, T. Mizushima, and K. Machida, Phys. Rev. A **81**, 063623 (2010).

[81] Y. Kawaguchi, H. Saito, and M. Ueda, Phys. Rev. Lett. **98**, 110406 (2007).

[82] D. V. Freilich, D. Bianchi, A. M. Kaufman, T. K. Langin, and D. S. Hall, Science **329**, 1182 (2010).

[83] L. Pitaevskii and S. Stringari, *Bose-Einstein Condensation* (Oxford Science Publications, Oxford, 2003).

[84] M. Ueda, *Fundamentals and New Frontiers of Bose-Einstein Condensation* (World Scientific, Singapore, 2010).

[85] A. E. Leanhardt, T. A. Pasquini, M. Saba, A. Schirotzek, Y. Shin, D. Kielpinski, D. E. Pritchard, and W. Ketterle, Science **301**, 1513 (2003).

[86] D. A. Steck, *Sodium D Line Data*, `http://steck.us/alkalidata` (revision 2.1.4, 23 December 2010).

[87] D. A. Steck, *Rubidium 87 D Line Data*, `http://steck.us/alkalidata` (revision 2.1.4, 23 December 2010).

[88] T. Ohmi and K. Machida, J. Phys. Soc. Jpn. **67**, 1822 (1998).

[89] T.-L. Ho, Phys. Rev. Lett. **81**, 742 (1998).

[90] O. Penrose and L. Onsager, Phys. Rev. **104**, 576 (1956).

[91] E. P. Gross, Nuovo Cimento **20**, 454 (1961).

[92] E. P. Gross, J. Math. Phys. **4**, 195 (1963).

[93] L. P. Pitaevskii, Zh. Éksp. Teor. Fiz. **40**, 646 (1961), [Sov. Phys. JETP **13**, 451 (1961)].

[94] W. H. Press, S. A. Teukolsky, W. T. Vetterling, and B. P. Flannery, *Numerical Recipes in FORTRAN: The Art of Scientific Computing* (Cambridge University Press, Cambridge, 1994).

[95] G. Strang, SIAM J. Numer. Anal. **5**, 506 (1968).

[96] T. Isoshima, K. Machida, and T. Ohmi, J. Phys. Soc. Jpn. **70**, 1604 (2001).

[97] T. Mizushima, K. Machida, and T. Kita, Phys. Rev. Lett. **89**, 030401 (2002).

[98] N. N. Bogoliubov, J. Phys. USSR **11**, 23 (1947).

[99] D. V. Skryabin, Phys. Rev. A **63**, 013602 (2000).

[100] M. Takahashi, V. Pietilä, M. Möttönen, T. Mizushima, and K. Machida, Phys. Rev. A **79**, 023618 (2009).

[101] A. L. Fetter, Ann. Phys. **70**, 67 (1972).

[102] M. Mine, M. Okumura, T. Sunaga, and Y. Yamanaka, Ann. Phys. **322**, 2327 (2007).

[103] A. M. Lyapunov, *Stability of Motion* (Academic Press, New York & London, 1966).

[104] R. S. MacKay, in *Hamiltonian Dynamical Systems*, edited by R. S. Kay and J. D. Meiss (Hilger, Bristol, 1987).

[105] L. Onsager, Nuovo Cimento **6**, Suppl. 2, 249 (1949).

[106] R. P. Feynman, in *Progress in Low Temperature Physics*, Vol. I, edited by C. J. Gorter and D. F. Brewer (North-Holland, Amsterdam, 1955).

[107] T.-L. Ho and V. B. Shenoy, Phys. Rev. Lett. **77**, 2595 (1996).

[108] A. A. Abrikosov, Zh. Éksp. Teor. Fiz. **32**, 1442 (1957).

[109] K. W. Madison, F. Chevy, W. Wohlleben, and J. Dalibard, Phys. Rev. Lett. **84**, 806 (2000).

[110] K. Madison, F. Chevy, W. Wohlleben, and J. Dalibard, J. Mod. Opt. **47**, 2715 (2000).

[111] C. Raman, J. R. Abo-Shaeer, J. M. Vogels, K. Xu, and W. Ketterle, Phys. Rev. Lett. **87**, 210402 (2001).

[112] J. R. Abo-Shaeer, C. Raman, J. M. Vogels, and W. Ketterle, Science **292**, 476 (2001).

[113] N. D. Mermin and T.-L. Ho, Phys. Rev. Lett. **36**, 594 (1976).

[114] T.-L. Ho, Phys. Rev. B **18**, 1144 (1978).

[115] A. E. Leanhardt, Y. Shin, D. Kielpinski, D. E. Pritchard, and W. Ketterle, Phys. Rev. Lett. **90**, 140403 (2003).

[116] J.-P. Martikainen, A. Collin, and K.-A. Suominen, Phys. Rev. A **66**, 053604 (2002).

[117] T. Mizushima, K. Machida, and T. Kita, Phys. Rev. A **66**, 053610 (2002).

[118] E. N. Bulgakov and A. F. Sadreev, Phys. Rev. Lett. **90**, 200401 (2003).

[119] T. Mizushima, N. Kobayashi, and K. Machida, Phys. Rev. A **70**, 043613 (2004).

[120] V. Pietilä, M. Möttönen, and S. M. M. Virtanen, Phys. Rev. A **76**, 023610 (2007).

[121] K. Maki and T. Tsuneto, J. Low Temp. Phys. **27**, 635 (1977).

[122] N. D. Mermin, Rev. Mod. Phys. **51**, 591 (1979).

[123] M. Nakahara, T. Isoshima, K. Machida, S.-I. Ogawa, and T. Ohmi, Physica B: Condens. Matter **284–288**, 17 (2000).

[124] T. Isoshima, M. Nakahara, T. Ohmi, and K. Machida, Phys. Rev. A **61**, 063610 (2000).

[125] S.-I. Ogawa, M. Möttönen, M. Nakahara, T. Ohmi, and H. Shimada, Phys. Rev. A **66**, 013617 (2002).

[126] M. Möttönen, N. Matsumoto, M. Nakahara, and T. Ohmi, J. Phys.: Condens. Matter **14**, 13481 (2002).

[127] Y. Kawaguchi, M. Nakahara, and T. Ohmi, Phys. Rev. A **70**, 043605 (2004).

[128] M. Kumakura, T. Hirotani, M. Okano, Y. Takahashi, and T. Yabuzaki, Phys. Rev. A **73**, 063605 (2006).

[129] V. Pietilä, M. Möttönen, and M. Nakahara, in *Electromagnetic, Magnetostatic, and Exchange Interaction Vortices in Confined Magnetic Structures*, edited by E. O. Kamenetskii (Transworld Research Network, Kerala, 2008).

[130] H. Shibayama, Y. Yasaku, and T. Kuwamoto, J. Phys. B: At. Mol. Opt. Phys. **44**, 075302 (2011).

[131] D. E. Pritchard, Phys. Rev. Lett. **51**, 1336 (1983).

[132] F. Zambelli and S. Stringari, Phys. Rev. Lett. **81**, 1754 (1998).

[133] F. Chevy, K. W. Madison, and J. Dalibard, Phys. Rev. Lett. **85**, 2223 (2000).

[134] Z. F. Xu, P. Zhang, C. Raman, and L. You, Phys. Rev. A **78**, 043606 (2008).

[135] Z. F. Xu, P. Zhang, R. Lü, and L. You, Phys. Rev. A **81**, 053619 (2010).

[136] M. V. Berry, Proc. R. Soc. A **392**, 45 (1984).

[137] T. P. Simula, S. M. M. Virtanen, and M. M. Salomaa, Phys. Rev. A **65**, 033614 (2002).

[138] Y. Shin, M. Saba, M. Vengalattore, T. A. Pasquini, C. Sanner, A. E. Leanhardt, M. Prentiss, D. E. Pritchard, and W. Ketterle, Phys. Rev. Lett. **93**, 160406 (2004).

[139] J. A. M. Huhtamäki, M. Möttönen, T. Isoshima, V. Pietilä, and S. M. M. Virtanen, Phys. Rev. Lett. **97**, 110406 (2006).

[140] M. Möttönen, T. Mizushima, T. Isoshima, M. M. Salomaa, and K. Machida, Phys. Rev. A **68**, 023611 (2003).

[141] A. Muñoz Mateo and V. Delgado, Phys. Rev. Lett. **97**, 180409 (2006).

[142] K. Gawryluk, M. Brewczyk, and K. Rzążewski, J. Phys. B: At. Mol. Opt. Phys. **39**, L225 (2006).

[143] N. R. Cooper, N. K. Wilkin, and J. M. F. Gunn, Phys. Rev. Lett. **87**, 120405 (2001).

[144] T. P. Simula, P. Engels, I. Coddington, V. Schweikhard, E. A. Cornell, and R. J. Ballagh, Phys. Rev. Lett. **94**, 080404 (2005).

[145] M. C. Davis, R. Carretero-González, Z. Shi, K. J. H. Law, P. G. Kevrekidis, and B. P. Anderson, Phys. Rev. A **80**, 023604 (2009).

[146] T. W. Neely, E. C. Samson, A. S. Bradley, M. J. Davis, and B. P. Anderson, Phys. Rev. Lett. **104**, 160401 (2010).

[147] S. I. Voropayev and Y. D. Afanasyev, *Vortex structures in a stratified fluid* (Chapman & Hall, London and New York, 1994).

[148] V. L. Berezinskii, Sov. Phys. JETP **32**, 493 (1971).

[149] V. L. Berezinskii, Sov. Phys. JETP **34**, 610 (1972).

[150] J. M. Kosterlitz and D. J. Thouless, J. Phys. C **5**, 124 (1972).

[151] J. M. Kosterlitz and D. J. Thouless, J. Phys. C **6**, 11181 (1973).

[152] V. Schweikhard, S. Tung, and E. A. Cornell, Phys. Rev. Lett. **99**, 030401 (2007).

[153] P. Cladé, C. Ryu, A. Ramanathan, K. Helmerson, and W. D. Phillips, Phys. Rev. Lett. **102**, 170401 (2009).

[154] M. Kobayashi and M. Tsubota, Phys. Rev. Lett. **94**, 065302 (2005).

[155] T.-L. Horng, C.-H. Hsueh, and S.-C. Gou, Phys. Rev. A **77**, 063625 (2008).

[156] E. A. L. Henn, J. A. Seman, G. Roati, K. M. F. Magalhães, and V. S. Bagnato, Phys. Rev. Lett. **103**, 045301 (2009).

[157] T. Frisch, Y. Pomeau, and S. Rica, Phys. Rev. Lett. **69**, 1644 (1992).

[158] T. Winiecki, J. F. McCann, and C. S. Adams, Phys. Rev. Lett. **82**, 5186 (1999).

[159] B. Jackson, J. F. McCann, and C. S. Adams, Phys. Rev. Lett. **80**, 3903 (1998).

[160] T. Winiecki, B. Jackson, J. F. McCann, and C. S. Adams, J. Phys. B: At. Mol. Opt. Phys. **33**, 4069 (2000).

[161] A. Ramanathan, K. C. Wright, S. R. Muniz, M. Zelan, W. T. Hill, C. J. Lobb, K. Helmerson, W. D. Phillips, and G. K. Campbell, Phys. Rev. Lett. **106**, 130401 (2011).

[162] L.-C. Crasovan, G. Molina-Terriza, J. P. Torres, L. Torner, V. M. Pérez-Garcia, and D. Mihalache, Phys. Rev. E **66**, 036612 (2002).

[163] L.-C. Crasovan, V. Vekslerchik, V. M. Pérez-Garcia, J. P. Torres, D. Mihalache, and L. Torner, Phys. Rev. A **68**, 063609 (2003).

[164] M. Möttönen, S. M. M. Virtanen, T. Isoshima, and M. M. Salomaa, Phys. Rev. A **71**, 033626 (2005).

[165] V. Pietilä, M. Möttönen, T. Isoshima, J. A. M. Huhtamäki, and S. M. M. Virtanen, Phys. Rev. A **74**, 023603 (2006).

[166] J. A. Seman, E. A. L. Henn, M. Haque, R. F. Shiozaki, E. R. F. Ramos, M. Caracanhas, P. Castilho, C. Castelo Branco, P. E. S. Tavares, F. J. Poveda-Cuevas, G. Roati, K. M. F. Magalhães, and V. S. Bagnato, Phys. Rev. A **82**, 033616 (2010).

[167] T. W. B. Kibble, J. Phys. A: Math. Gen. **9**, 1387 (1976).

[168] W. H. Zurek, Nature **317**, 505 (1985).

[169] V. M. H. Ruutu, V. B. Eltsov, A. J. Gill, T. W. B. Kibble, M. Krusius, Y. G. Makhlin, B. Placais, G. E. Volovik, and W. Xu, Nature **382**, 334 (1996).

[170] V. B. Eltsov, T. W. B. Kibble, M. Krusius, V. M. H. Ruutu, and G. E. Volovik, Phys. Rev. Lett. **85**, 4739 (2000).

[171] C. N. Weiler, T. W. Neely, D. R. Scherer, A. S. Bradley, M. J. Davis, and B. P. Anderson, Nature **455**, 948 (2008).

[172] W. Li, M. Haque, and S. Komineas, Phys. Rev. A **77**, 053610 (2008).

[173] S. Middelkamp, P. G. Kevrekidis, D. J. Frantzeskakis, R. Carretero-González, and P. Schmelcher, Phys. Rev. A **82**, 013646 (2010).

[174] J. Stockhofe, S. Middelkamp, P. Schmelcher, and P. G. Kevrekidis, Eur. Phys. Lett. **93**, 20008 (2011).

[175] S. Middelkamp, P. J. Torres, P. G. Kevrekidis, D. J. Frantzeskakis, R. Carretero-González, P. Schmelcher, D. V. Freilich, and D. S. Hall, Phys. Rev. A **84**, 011605 (2011).

[176] K. Kasamatsu, M. Tsubota, and M. Ueda, Int. J. Mod. Phys. B **19**, 1835 (2005).

[177] K. Kasamatsu, M. Tsubota, and M. Ueda, Phys. Rev. Lett. **93**, 250406 (2004).

[178] K. Kasamatsu, M. Tsubota, and M. Ueda, Phys. Rev. A **71**, 043611 (2005).

[179] K. Kasamatsu and M. Tsubota, Phys. Rev. A **79**, 023606 (2009).

[180] S.-J. Yang, Q.-S. Wu, S.-N. Zhang, and S. Feng, Phys. Rev. A **77**, 033621 (2008).

[181] P. Mason and A. Aftalion, Phys. Rev. A **84**, 033611 (2011).

[182] E. J. Mueller and T.-L. Ho, Phys. Rev. Lett. **88**, 180403 (2002).

[183] K. Kasamatsu, M. Tsubota, and M. Ueda, Phys. Rev. Lett. **91**, 150406 (2003).

[184] M. Keçeli and M. Ö. Oktel, Phys. Rev. A **73**, 023611 (2006).

[185] E. K. Dahl, E. Babaev, and A. Sudbø, Phys. Rev. Lett. **101**, 255301 (2008).

[186] M. P. Mink, C. M. Smith, and R. A. Duine, Phys. Rev. A **79**, 013605 (2009).

[187] J. A. M. Huhtamäki, T. P. Simula, M. Kobayashi, and K. Machida, Phys. Rev. A **80**, 051601 (2009).

[188] G. Ferrari, M. Inguscio, W. Jastrzebski, G. Modugno, G. Roati, and A. Simoni, Phys. Rev. Lett. **89**, 053202 (2002).

[189] G. Modugno, M. Modugno, F. Riboli, G. Roati, and M. Inguscio, Phys. Rev. Lett. **89**, 190404 (2002).

[190] J. Catani, L. De Sarlo, G. Barontini, F. Minardi, and M. Inguscio, Phys. Rev. A **77**, 011603 (2008).

[191] G. Thalhammer, G. Barontini, L. De Sarlo, J. Catani, F. Minardi, and M. Inguscio, Phys. Rev. Lett. **100**, 210402 (2008).

[192] K. Aikawa, D. Akamatsu, J. Kobayashi, M. Ueda, T. Kishimoto, and S. Inouye, New J. Phys. **11**, 055035 (2009).

[193] S. B. Papp, J. M. Pino, and C. E. Wieman, Phys. Rev. Lett. **101**, 040402 (2008).

[194] S. Sugawa, R. Yamazaki, S. Taie, and Y. Takahashi, Phys. Rev. A **84**, 011610 (2011).

[195] A. Lercher, T. Takekoshi, M. Debatin, B. Schuster, R. Rameshan, F. Ferlaino, R. Grimm, and H.-C. Nägerl, Eur. Phys. J. D **65**, 3 (2011).

[196] V. Schweikhard, I. Coddington, P. Engels, S. Tung, and E. A. Cornell, Phys. Rev. Lett. **93**, 210403 (2004).

[197] C. J. Myatt, E. A. Burt, R. W. Ghrist, E. A. Cornell, and C. E. Wieman, Phys. Rev. Lett. **78**, 586 (1997).

[198] D. S. Hall, M. R. Matthews, J. R. Ensher, C. E. Wieman, and E. A. Cornell, Phys. Rev. Lett. **81**, 1539 (1998).

[199] G. Delannoy, S. G. Murdoch, V. Boyer, V. Josse, P. Bouyer, and A. Aspect, Phys. Rev. A **63**, 051602 (2001).

[200] R. P. Anderson, C. Ticknor, A. I. Sidorov, and B. V. Hall, Phys. Rev. A **80**, 023603 (2009).

[201] R. Barnett, G. Refael, M. A. Porter, and H. P. Büchler, New J. Phys. **10**, 043030 (2008).

[202] R. Barnett, E. Chen, and G. Refael, New J. Phys. **12**, 043004 (2010).

[203] C. Chin, R. Grimm, P. Julienne, and E. Tiesinga, Rev. Mod. Phys. **82**, 1225 (2010).

[204] C. A. Stan, M. W. Zwierlein, C. H. Schunck, S. M. F. Raupach, and W. Ketterle, Phys. Rev. Lett. **93**, 143001 (2004).

[205] S. Inouye, J. Goldwin, M. L. Olsen, C. Ticknor, J. L. Bohn, and D. S. Jin, Phys. Rev. Lett. **93**, 183201 (2004).

[206] K. Pilch, A. D. Lange, A. Prantner, G. Kerner, F. Ferlaino, H.-C. Nägerl, and R. Grimm, Phys. Rev. A **79**, 042718 (2009).

[207] S. Tung, V. Schweikhard, and E. A. Cornell, Phys. Rev. Lett. **97**, 240402 (2006).

[208] J. Doyle, B. Friedrich, R. V. Krems, and F. Masnou-Seeuws, Eur. Phys. J. D **31**, 149 (2004).

[209] S. Ospelkaus, A. Pe'er, K.-K. Ni, J. J. Zirbel, B. Neyenhuis, S. Kotochigova, P. S. Julienne, J. Ye, and D. S. Jin, Nature Phys. **4**, 622 (2008).

[210] K.-K. Ni, S. Ospelkaus, M. H. G. de Miranda, A. Pe'er, B. Neyenhuis, J. J. Zirbel, S. Kotochigova, P. S. Julienne, D. S. Jin, and J. Ye, Science **322**, 231 (2008).

[211] J. Deiglmayr, A. Grochola, M. Repp, K. Mörtlbauer, C. Glück, J. Lange, O. Dulieu, R. Wester, and M. Weidemüller, Phys. Rev. Lett. **101**, 133004 (2008).

[212] A. Griesmaier, J. Werner, S. Hensler, J. Stuhler, and T. Pfau, Phys. Rev. Lett. **94**, 160401 (2005).

[213] P. O. Fedichev, Y. Kagan, G. V. Shlyapnikov, and J. T. M. Walraven, Phys. Rev. Lett. **77**, 2913 (1996).

[214] M. Theis, G. Thalhammer, K. Winkler, M. Hellwig, G. Ruff, R. Grimm, and J. H. Denschlag, Phys. Rev. Lett. **93**, 123001 (2004).

[215] Q. Beaufils, R. Chicireanu, T. Zanon, B. Laburthe-Tolra, E. Maréchal, L. Vernac, J.-C. Keller, and O. Gorceix, Phys. Rev. A **77**, 061601 (2008).

[216] K. Góral and L. Santos, Phys. Rev. A **66**, 023613 (2002).

[217] L. Santos, G. V. Shlyapnikov, and M. Lewenstein, Phys. Rev. Lett. **90**, 250403 (2003).

[218] G. Bismut, B. Pasquiou, E. Maréchal, P. Pedri, L. Vernac, O. Gorceix, and B. Laburthe-Tolra, Phys. Rev. Lett. **105**, 040404 (2010).

[219] M. Abraham, I. Aranson, and B. Galanti, Phys. Rev. B **52**, R7018 (1995).

[220] I. Aranson and V. Steinberg, Phys. Rev. B **53**, 75 (1996).

[221] N. N. Klausen, J. L. Bohn, and C. H. Greene, Phys. Rev. A **64**, 053602 (2001).

[222] H. Schmaljohann, M. Erhard, J. Kronjäger, M. Kottke, S. van Staa, L. Cacciapuoti, J. J. Arlt, K. Bongs, and K. Sengstock, Phys. Rev. Lett. **92**, 040402 (2004).

[223] M.-S. Chang, C. D. Hamley, M. D. Barrett, J. A. Sauer, K. M. Fortier, W. Zhang, L. You, and M. S. Chapman, Phys. Rev. Lett. **92**, 140403 (2004).

[224] M. Takahashi, T. Mizushima, M. Ichioka, and K. Machida, Phys. Rev. Lett. **97**, 180407 (2006).

[225] M. Lu, N. Q. Burdick, S. H. Youn, and B. L. Lev, Phys. Rev. Lett. **107**, 190401 (2011).

[226] V. N. Popov, *Functional Integrals and Collective Excitations* (Cambridge University Press, Cambridge, 1990).

[227] A. Griffin, Phys. Rev. B **53**, 9341 (1996).

[228] P. B. Blakie, A. S. Bradley, M. J. Davis, R. J. Ballagh, and C. W. Gardiner, Adv. Phys. **57**, 363 (2008).

[229] E. Zaremba, T. Nikuni, and A. Griffin, J. Low Temp. Phys. **116**, 227 (1999).

In 1995, the field of atomic physics took a quantum leap with the experimental discovery of dilute Bose-Einstein condensates in trapped atomic gases. The dilute condensates offer a chance to study an interacting many-particle system accurately from first-principles theories, and they can be used to simulate many seminal models that have proven elusive in their original context of, e.g., solid-state or high-energy physics. An important topic in the research has been the quantized vortex, which was experimentally realized in 1999 and whose existence is intimately related to the concepts of superfluidity and quantum phase coherence. In this dissertation, unconventional vortex structures are investigated in the trapped condensates using a combination of analytical and numerical methods. Several results are reported that contribute to a better understanding of superfluid phenomena and have significant implications for the prospects of detecting novel vortex structures in current experiments.

Aalto-DD 118/2012

ISBN 978-952-60-4784-3
ISBN 978-952-60-4785-0 (pdf)
ISSN-L 1799-4934
ISSN 1799-4934
ISSN 1799-4942 (pdf)

Aalto University
School of Science
Department of Applied Physics
www.aalto.fi